AD-A048 603 NATIONAL SEVERE STORMS LAB NORMAN OKLA F/G 4/2
APPLICATION OF DOPPLER WEATHER RADAR TO TURBULENCE MEASUREMENTS--ETC(U)
MAR 77 J T LEE DOT-FA74WAI-495
UNCLASSIFIED NSSL-1 FAA/RD-77/145 NL

END
DATE FILMED
2-78
DDC

Report No. FAA-RD-77-145

APPLICATION OF DOPPLER WEATHER RADAR TO TURBULENCE MEASUREMENTS WHICH AFFECT AIRCRAFT

J.T. Lee
National Severe Storms Laboratory
National Oceanic and Atmospheric Administration
Department of Commerce
1313 Halley Circle
Norman, Oklahoma 73069

March 1977
Final Report

Prepared for

U.S. DEPARTMENT OF TRANSPORTATION
FEDERAL AVIATION ADMINISTRATION
Systems Research & Development Service
Washington, D.C. 20590

(18) FAA/RD (19) 77/145

Technical Report Documentation Page

1. Report No.	2. Government Accession No.	3. Recipient's Catalog No.
FAA-RD-77-145 ✓		

(6) 4. Title and Subtitle: Application of Doppler Weather Radar to Turbulence Measurements Which Affect Aircraft.

(11) 5. Report Date: [illegible]77 (12) 52p.

(14) 6. Performing Organization Code: NSSL-1

8. Performing Organization Report No.

(10) 7. Author(s): J. T./Lee

9. Performing Organization Name and Address:
National Severe Storms Laboratory
1313 Halley Circle
Norman, Oklahoma 73069 ✓

10. Work Unit No. (TRAIS)

(15) 11. Contract or Grant No.: DOT-FA 74WAI-495 new

(9) 13. Type of Report and Period Covered: FINAL REPORT.

12. Sponsoring Agency Name and Address:
U.S. Department of Transportation
Federal Aviation Administration
* Systems Research and Development Service
Washington, D.C. 20590 ✓

14. Sponsoring Agency Code: ARD-450

15. Supplementary Notes

* Aviation Weather Branch.

16. Abstract

Analysis of thunderstorm turbulence hazardous to aircraft operation and coordinated Doppler radar observations indicate a high potential for Doppler radar utilization particularly the mean velocity spectrum breadth observations in defining severe turbulence areas. The Mean Velocity Processor (MVP, the first real-time display of Doppler radar data) and the Multi-moment Ling Display (MMD), both developed at NSSL, are utilized with the radars to study vortex motion, turbulence, and wind shear areas. In addition, the Plan Shear Indicator (PSI) developed by the Air Force Cambridge Research Laboratory (AFCRL) was also employed. A number of severe convective storms were penetrated by an instrumented aircraft directed into areas which analysis inferred to be turbulent. Aircraft recorded turbulence and concurrent Doppler data are compared. Utilization of the spectrum breadth calculated from the mean velocity data as a turbulence "signature" is discussed. Vortex motion "signature" is also defined.

17. Key Words	18. Distribution Statement
Thunderstorm Turbulence Doppler Radar Radar Displays	Document is available to the U.S. public through the National Technical Information Service, Springfield, Virginia 22161.

19. Security Classif. (of this report)	20. Security Classif. (of this page)	21. No. of Pages	22. Price
UNCLASSIFIED	UNCLASSIFIED	52	

Form DOT F 1700.7 (8-72) Reproduction of completed page authorized

244 67¢

PREFACE

This final report relates to the investigation of Doppler radar techniques for real-time display of wind velocities in storms and measurements of parameters which correlate well with turbulence hazardous to aircraft operation. This report presents the state-of-the-art in Doppler radar as it applies to convective weather and aircraft operations.

A work summary leading to a real-time display of Doppler measured velocity data is presented. Detailed also is the coordinated measurements of thunderstorm turbulence using aircraft and Doppler radar. Mesocyclone and tornado vortex recognition signatures are described.

Meteorological Doppler radar possibly represents the most significant new capability for identification and avoidance of dangerous weather conditions associated with thunderstorms since introduction of standard weather radar.

The work presented herein represents the cumulative effort of the staff at NSSL and cooperating agencies. Particular mention is made of Dr. Richard Doviak, Mr. Dale Sirmans and Mr. Larry Hennington for their contribution to the Doppler and real-time displays and Messrs. Donald Burgess, Rodger Brown and Leslie Lemon in the vortex identification.

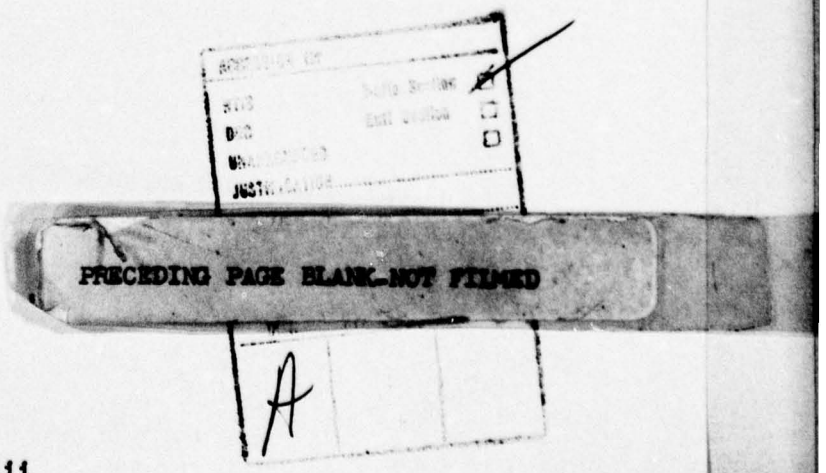

TABLE OF CONTENTS

LIST OF FIGURES

APPLICATION OF DOPPLER WEATHER RADAR TO TURBULENCE MEASUREMENTS WHICH AFFECT AIRCRAFT

1. INTRODUCTION

1.1 Nature of the Problem

Thunderstorms represent a major hazard to aircraft operations. Because of thunderstorms, large sections are removed from air space otherwise available to aircraft, with accompanying disruption of service and increased cost and energy consumption. At times, airports may be closed to traffic for tens of minutes or aircraft detoured hundreds of miles to avoid thunderstorm systems. FAA Circular 00-24 addresses problems of thunderstorm avoidance. Use of improved diagnostic techniques for warning of severe thunderstorm hazards would improve flight safety and increase usable air space.

1.2 Objectives and Scope of Study

The development of Doppler radar offers the first practical method for measuring wind fields in detail inside storms and for virtually continuous profiling of the horizontal wind at various altitudes. Identifiable wind features should be related to turbulent areas and other hazards such as wind shear. This study emphasizes thunderstorms and has objectives: (1) to develop methods for real-time display of Doppler wind data and other parameters in a manner easily interpreted and; (2) to determine hazards represented by these data. Signal processing and display techniques were developed and utilized with coordinated aircraft measurements of suspected turbulent areas. The following sections relate progress.

2. DOPPLER RADAR SIGNAL PROCESSING

Radar echo intensity and Doppler velocity must be considered together in analysis and application.

Recent advances in integrated circuits and accompanying reduction of cost for digital equipment has led to NSSL's present digital integrator for echo intensity (reflectivity) measurements (Fig. 1-1). This is generally superior in performance, more stable, simpler, more reliable, and less costly than analogue systems now in operational use. In addition, the digital system offers more versatility in data handling, with output data fed to both a magnetic tape recorder and to a PPI scope for real-time interpretation (Fig. 1-2).

2.1 Mean Velocity Processor

Real-time display of Doppler radar velocity data has also been investigated.

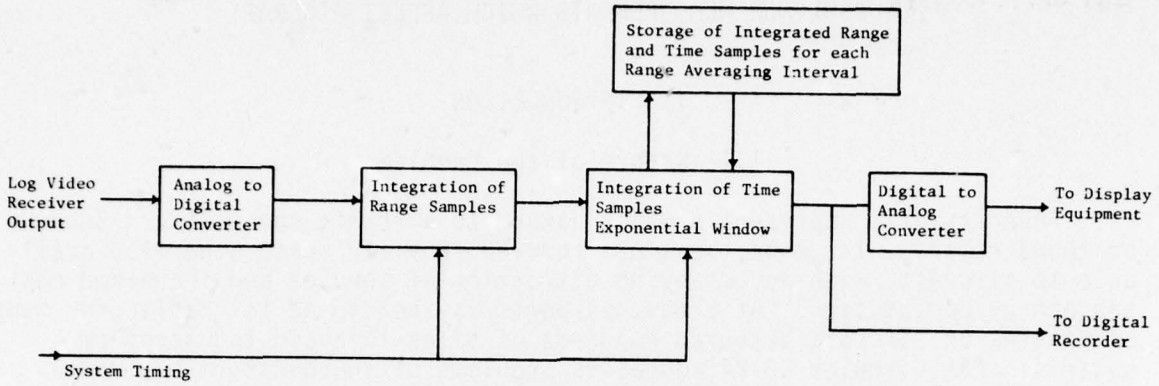

Figure 1-1. Digital integrator block diagram.

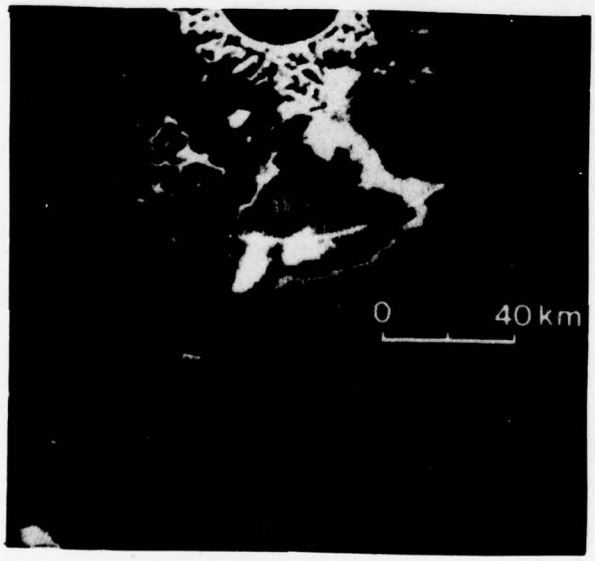

Figure 1-2. Contoured display of the WSR-57 radar echo (>10 dBz) of the Davis Storm at 1700 CST. Antenna elevation is 0 deg.

The "Mean Velocity Processor" (MVP) [originally called "Octant Change Counter" (OCC)] (Sirmans, 1973) provides an estimate of the mean velocities of meteorological targets simultaneously at 200 range locations along a radial. It is the first device in the world to provide a contour-mapped PPI display of meteorological target velocities in real time. The MVP processing rate is commensurate with the radar output data rate, and mean velocity estimates are acquired in a time limited only by the desired estimate accuracy. This system estimates mean velocities at multiple pulse volumes along a radial while circumventing spectral calculations and large-scale storage by acting on pairs of complex time samples to compute the echo scalar phase change over a pulse repetition period. Each calculated phase is compared with the previous phase and the quantized displacements from consecutive pulses are stored. The consecutive displacements are summed algebraically for a fixed number of pulse pairs; the expected net displacement

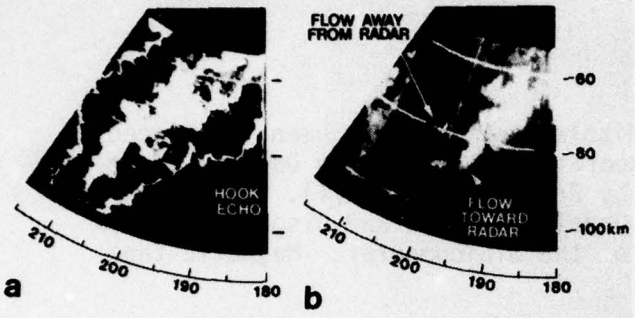

Figure 1-3. PPI reflectivity (A) and Doppler isotachs (B) at 2115 CST. The elevation angle is 1.9°, RM 60, 80, 100 km. Reflectivity categories are dim (<21 dBz), bright (21-31), black (31-44), dim (44-57), and bright (>57 dBz). Velocity categories are dim (<13 m sec^{-1}), bright (13-21), and brightest (>21 m sec^{-1}). Positive radial velocities are angularly strobed. Mesocyclone type signature at 198°/82 km.

is proportional to the mean velocity in the sampling volume. A sample simultaneous display of mean echo intensity and Doppler velocity estimate in a PPI mode is shown in Figure 1-3.

Doppler radar measurements in severe storms are significantly limited by a relationship between the maximum unambiguous range R_a and the maximum unambiguously resolved radial velocity $|V_m|$ (i.e. the Nyquist limit). This is defined by the equations $|V_m| = 2(PRF)\,\lambda/8$ and $R_a = C/2\,PRF$ where C is the speed of light, λ is the radar wavelength, and PRF is the pulse repetition frequency. Thus for a given radar, increasing PRF to give a greater velocity interval results in decreased range. The study by Doviak and Sirmans (1973) suggests use of horizontal and vertical polarization with pulse-pair processing to extend the range of velocities measurable with a specified PRF. The proposal merits further study.

Further investigation of pulse-pair processing techniques is also required to obtain more complete information from a singly polarized system. A system that calculates the vector phase change rather than the scalar change between successive pulses provides more accurate velocity estimates than the MVP when velocities are near the Nyquist limit, and is described on page 6 below.

2.2 Multimoment Display

Doppler radar provides, in addition to the precipitation echo spectrum power (zeroth moment)--which is proportional to reflectivity (Z)--and the mean Doppler velocity (first moment), the velocity spread or spectrum broadness, B, (second moment about the mean) of precipitation particles within the pulse volume.

Integration of these three spectrum characteristics into a single display provides superior real-time information for decision making.

The display developed in 1974 is described by Burgess et al. (1976) as follows:

Display Description

A minicomputer-graphic display terminal has been interfaced to a National Severe Storm Laboratory (NSSL) 10 cm Doppler radar having characteristics given by Brown et al. (1971). The algorithms necessary to estimate Doppler moments and display controls are accomplished through use of the minicomputer. Magnetic tape also records displayed data.

To simultaneously present the three principal Doppler moments for each pulse volume, a field of arrows is displayed where arrow length is proportional to the log of received power, arrow direction to velocity and arrowhead size to Doppler spectrum width. For examples presented here, arrowhead size is programmed to be proportional to Doppler wind shear, a significant contributor to spectrum width.

Figure 2-1 illustrates the above relations. Zero velocity is a horizontal arrow pointing right and nonzero velocities are proportional to the angle between the arrow and its zero position. Clockwise rotation from the zero position denotes negative velocities (toward the radar) and counterclockwise rotation denotes positive velocities (away from the radar). The horizontal arrow pointing left corresponds to the maximum unambiguous velocity (±34 m s^{-1}) resolved by the radar. As the velocity increases beyond ±34 m s^{-1}, the arrow rotates smoothly and appears as a lower velocity of opposite sign (e.g., 38 m s^{-1} appears as -30 m s^{-1}). Arrowhead width reflects the largest absolute velocity difference between the sample volume under consideration

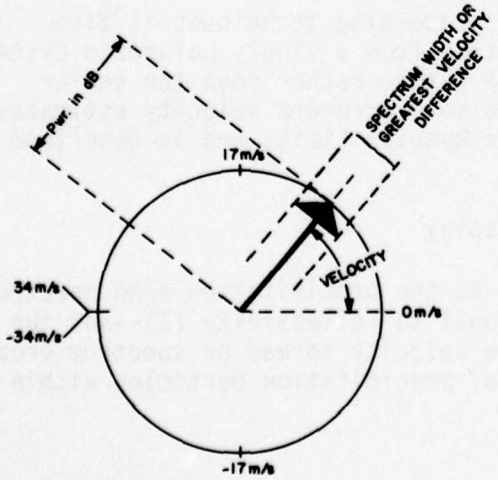

Figure 2-1. Relationships between display arrows and the three Doppler moments. Arrow length is proportional to received power, arrow direction to velocity and arrowhead size to Doppler spectrum width or velocity difference.

and the four surrounding volumes. Due to the limited unambiguous velocity, the velocity difference is computed by

$$\Delta V = \begin{cases} |V_1 - V_2| & \text{when } |V_1 - V_2| \leq 34 \text{ m s}^{-1} \\ 68 - |V_1 - V_2| & \text{when } |V_1 - V_2| \geq 34 \text{ m s}^{-1} \end{cases}$$

to eliminate the potential for large numbers of erroneous differences across the maximum unambiguous velocity. Therefore, the difference between +30 and -28 m s^{-1} is displayed as 10 m s^{-1}, not 58 m s^{-1}. Unfortunately, real velocity differences >34 m s^{-1} are ignored in arrowhead size but arrow direction may still be used to correctly interpret large velocity differences.

The display (Fig. 2-2) is a B-SCAN (range vs. azimuth) presentation of Doppler moments where ranges in kilometers and azimuths in degrees are given along the left and bottom margins, respectively. Top headers show time, radar elevation angle, kilometer range interval (dR) and kilometer azimuth interval (dAZ) between whole degrees. The display sector is limited to 15 x 16 pulse volumes but range and azimuth spacing between displayed pulse volumes is variable and the sector limits can be changed quickly. Thus it is possible to check large storm regions for severe storm signatures. A variable minimum power threshold is used to separate noise from regions where velocity estimates may be obtained. For the examples shown, a signal-to-noise ratio of 3.5 dB is used as the boundary for displayed data.

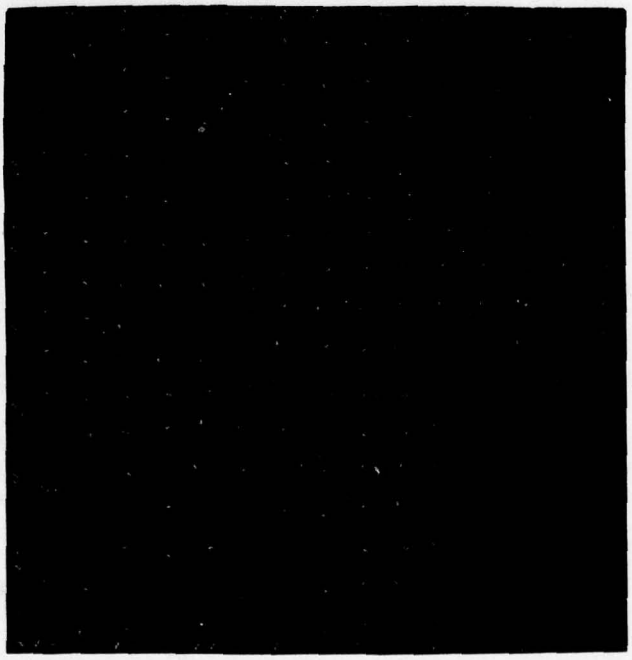

Figure 2-2 Multimoment display for Stillwater storm of 13 June 1975 before tornado formation. Time, elevation angle, range interval (dR) and azimuth interval (dAZ) at the nearest range between arrows are given across display top. Mesocyclone center is indicated by (+).

Velocities are computed using the pulse pair technique to determine spectral moments from signal covariance (Berger and Groginsky, 1973). To reduce computational time, alternate sample pairs (e.g., samples 1 and 2, 5 and 6, etc.) are processed to obtain, from 64 uniformly spaced samples, 16 pulse pairs to estimate Doppler moments. The standard error of velocity estimates is about 0.7 m s^{-1} for spectra width equal to 3 m s^{-1}, a typical value. The use of alternate pairs results in a negligible increase of variance over that predicted by Berger and Groginsky if the full 63 sample pairs were processed.[2] These errors are within the accuracy expected when interpreting the velocity displays and are considered reasonable for real time use.

This display is very effective and, beginning in 1975, is used in the decision making processes whenever penetration aircraft are flying.

2.3 Plan-Shear Indicator

A third type of display, the Plan-Shear Indicator (PSI) developed by the then Air Force Cambridge Research Laboratory (AFCRL) (Armstrong and Donaldson, 1969) was also tested. This is discussed in detail by Lee and Kraus (1975). The PSI display (Fig. 2-3) indicates shear by a differential displacement of adjacent precipitation targets producing "wiggles" in the display. The width of the concentric area is proportional to the second movement. However the scale factor did not permit use of this characteristic. Results using these displays are detailed in the next section.

3. PLAN-SHEAR INDICATOR AND AIRCRAFT MEASUREMENTS OF THUNDERSTORM TURBULENCE

A Doppler experiment Spring 1973, in Oklahoma, involved Air Force Cambridge Research Laboratories (AFCRL, presently Air Force Geophysical Laboratory), Aeronautical Systems' Division (ASD), Federal Aviation Administration (FAA), Colorado State University (CSU) and National Severe Storms Laboratory (NSSL).

3.1 Test Operation

The NSSL Doppler radar, Norman, Oklahoma was modified to operate in either the PSI or standard mode since the differing requirements on pulse repetition frequency of the two systems did not permit simultaneous operations. During a portion of the program, the radar was alternated between the two modes for a series of penetrations by instrumented aircraft.

Ground clutter out to 38 km and second trip considerations limited alternate sampling operations to ranges from 38 km to 114 km and from 152 km to 164 km, substantially reducing the number of opportunities for comparisons.

---

[2] Private communication, Dr. Dusan Zrnic, a visiting scientist at the National Severe Storms Laboratory.

When a storm with intensity larger than 30 dBZ approached or appeared within the acceptable ranges, aircraft were launched and vectored to the storm area avoiding reflectivities zones greater than 50 dBZ where damaging hail is common (Burnham and Lee, 1969).

The PSI Doppler scope was viewed for indications of shear. When a shear area was observed, (wiggles present) the aircraft was vectored through the area. Aircraft tracking was accomplished with transponder data fed into the WSR-57 10-cm weather radar system and displayed simultaneously with contours of radar echo reflectivity. This photographed display provides an aircraft position every 20 seconds. For analysis, straight line interpolation was used between each recorded position (Fig. 3-1). WWV time signals were used to coordinate aircraft, weather radar, Doppler radar, and voice data. A 1 km radius circle of error is probable. Aircraft data were recorded at 50 per second and a five-point smoothed average provided 0.1 s values for computation of true vertical velocities (w) and, as a measure of turbulence, derived gust velocities (U_{de}) (Hombolt, et al, 1964). The penetration true airspeed was approximately 170 m s^{-1} with the F-100, 210 m s^{-1} with the F-101. Thus 0.1 s data points correspond to observations about every 20 m. The PSI has a range resolution of 855 m and the 0.8° beam width provides an azimuthal resolution of about 1.1 km at 80 km. Hence, we are concerned with turbulent encounters of several seconds or more. More specifically, the 0.1 s aircraft data output corresponds to a maximum unambiguous frequency (f_{max}) of 5 Hz and a corresponding minimum wavelength (L_{min}) along the flight path represented by

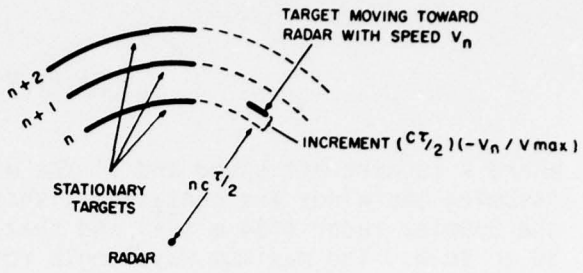

Figure 2-3. PSI display for stationary targets (left) and a moving target (right). The moving target is located at the same distance from the radar as the nearest stationary target, but is displaced from it on the PSI display by an increment which depends on its velocity (Armstrong and Donaldson, 1969).

Figure 3-1. 16 June 1973, WSR-57 weather radar reflectivity isoecho contours display with aircraft transponder beacons superimposed. Point A is the beacon return from the F-100 at 1357:25 CST; the dotted line indicates aircraft path. Range marks, at 40 km intervals.

$$L_{min} = (V \pm V')(f_{max})^{-1}$$

where V is aircraft speed and V' the wind speed along the flight path. Assuming the winds are contained within the maximum unambiguous velocity of the Doppler radar (± 34 m s^{-1}) and that the Taylor hypothesis holds, L_{min} is 30 to 40 m. The maximum wavelength resolvable is equipment dependent and is estimated to be about 2000 m (Ryan et al., 1971).

In the Doppler data field, L_{min} is dependent on range and aspect angle due to radar beam divergence and differences between range and angular resolution. In the series of complete Doppler spectrum data, the range sampling interval of 300 m yields L_{min} = 600 m if the aircraft flies along a radar beam. At the working distance of 60 km, the 0.8° beam width provides L_{min} of about 1600 m. Data obtained within a pulse volume are the product of several integrated factors throughout the total volume which is quite large (3.308×10^8 m^3 at 60 km) and it is difficult to resolve turbulent wavelengths within the volume. Thereby we see that pattern correspondence rather than point-to-point correspondence must be utilized in correlation studies.

Another consideration is that the Doppler primarily measures the horizontal wind component at low elevation angles used for PPI-type displays. With aircraft, the vertical component is measured. However, Houbolt et al., (1964), Ashburn et al., (1970) and others have shown that turbulence affecting aircraft above the boundary layer is mainly isotropic, particularly so in convective clouds. This we assumed in the present study.

The F-101 made penetration on 6 days (Table 3-1); not all data from these flights are available. The F-100 aircraft penetrated thunderstorms on five days. On three of these days (12 penetrations) it was possible to compare PSI presentation and U_{de}. Derived gust velocities were divided into four categories as shown in Table 3-2. When the aircraft recorded only light turbulence or less, the PSI arcs were smooth, for example 15 June F 1R1 and 16 June F 1R5 (Table 3-3).

TABLE 3-1

Aircraft Operation Days when PSI Data Recorded

F-101	F-100
26 April 1973	1 June 1973
6 May	4
21	11
23	15
26	16
1 June	

TABLE 3-2

Interval	Approximate Turbulence Class (NASA)
$3.0 \leq U_{de} \leq 6.0$ m s^{-1} (10-19 ft s^{-1})	Light
$6.1 \leq U_{de} \leq 9.1$ m s^{-1} (20-29 ft s^{-1})	Moderate
$9.2 \leq U_{de} \leq 12.1$ m s^{-1} (30-39 ft s^{-1})	Severe
$U_{de} \geq 12.2$ m s^{-1} ($\geq$ 40 ft s^{-1})	Extreme

TABLE 3-3

Date (1973) and Flight	Time(s) in Turbulence		PSI Display
	Cat. B (MDT)	Cat. C (SVR)	
4 June F 1R5	<1	0	Smooth
15 June F 1R1	0	0	Smooth
F 2R1	2.8	0.3	Small wiggles
F 2R3	5	0	Smooth
16 June F 1R3	23	1	Smooth
F 1R4	13.4	0.6	Smooth
F 1R5	0	0	Smooth
F 1R6	11	0.5	Wiggles
16 June F 2R1	79	1.8	Wiggles
F 2R2	14	5.0	Smooth (Dim Photo)
F 2R3	8	0.6	Wiggles
F 2R4	5	0	Smooth

Other turbulence categories did not exhibit as good a correlation. Moderate turbulence was encountered on ten penetrations. Seven of these also contained 0.3 s or longer embedded severe turbulence areas. Example: on 16 June the PSI indicated radial wind shear during penetrations 1 (Fig. 3-2) and 3 of the second flight. In both cases, severe turbulence (Fig. 3-3) was encountered in the vicinity of the wiggles. However, there was no indication of shear along the flight path in the moderate turbulence area preceding the severe turbulence. For the second run of the same series (F 2R2) the PSI data appeared to show no high shears in the severe turbulence areas. In the moderate turbulence encounter areas there was no evidence of wiggles.

15 June F 2R1 and F 2R3 had areas in which the U_{de}'s indicated moderate turbulence and in F 2R1 a short burst of severe turbulence. Along the aircraft track the PSI's for both flights were smooth. A small area of weak shear was indicated on the PSI about 10 km SW of the point where the aircraft experienced some moderate turbulence--not apparently related to the aircraft encounter.

16 June, F 1R3 was associated with a smooth PSI although relatively long periods of moderate turbulence, and a short period of severe, were recorded. On F 1R4 once again the PSI showed no wiggles along the flight track but did indicate some shear 10 km NNE of the severe turbulence encounter.

On F 1R6 of the same day there is an area of shear along the flight path very close to the location where the aircraft measured severe turbulence. However, at the time of the PSI photo (2 minutes before the turbulence encounter time) the location of shear is several thousand feet higher than the aircraft location. Closer to the aircraft altitude, but a minute or two earlier indication of shear was debatable.

Table 3-2 summarizes PSI indicators and turbulence experienced during penetrations for all full data set cases. An example of vertical velocities encountered is shown by the time history (Fig. 3-4) calculated from F-101 data for 26 May 1973.

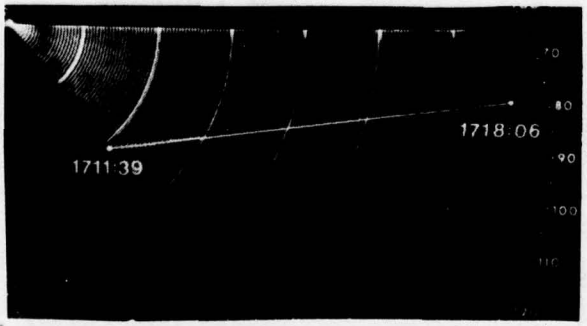

Figure 3-2. PSI for 1710 CST 16 June 1973. 4° tilt. 20 km range marks.

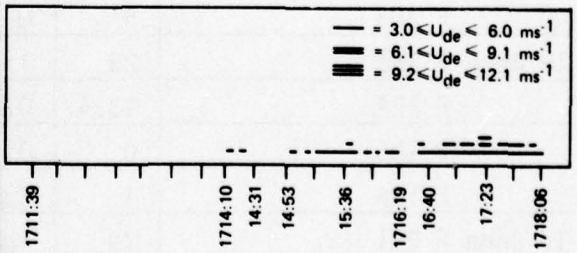

Figure 3-3. Penetration track time and turbulence intensities encountered corresponds to flight in Figure 4.

3.2 Summary

Moderate or severe turbulence was encountered in all cases when the PSI displayed wiggles along the aircraft flight path, but wiggles were not present with all turbulence encounters. Thus, it appears from these cases that turbulence up through moderate ($U_{de} \leq 9.1$ m s^{-1}) may escape detection by the PSI. Where severe turbulence ($U_{de} \geq 9.1$ m s^{-1}) repeatedly was encountered, the PSI showed transient (less than one minute duration) shear areas along the flight path. Arc deformations apparently have an operational detectability threshold associated with wind shears $\geq 1.5 \times 10^{-2}$ s^{-1}.

4. DUAL DOPPLER AND SINGLE DOPPLER OBSERVATIONS AND CONCURRENT AIRCRAFT THUNDERSTORM PENETRATIONS

4.1 General

In 1974 an F-4-C aircraft replaced the F-100, a second Doppler radar was installed at Cimarron Airport, Oklahoma City, Oklahoma and as noted in Section 2.2 the multi-moment display was available. The second Doppler used in conjunction with the Norman unit makes possible the calculation of winds within a thunderstorm. The second Doppler also permits comparison of thunderstorm parameters as seen from different viewing angles. Operational procedures remained essentially the same as detailed in Section 3.1. Average penetration airspeed for the F-4-C is 150 m s^{-1}. The F-4-C was on station at Tinker AFB, Oklahoma (TIK) from 15 April through 29 April 1974 and 15 May through 30 May 1974. Eight flights were made during this time; dates and penetration altitude are shown in Table 4-1. Penetration altitudes are as low as possible to reduce contamination of the Doppler velocity by vertical velocities associated with falling precipitation. In 1975 the aircraft was available 18 May through 10 June and nine flights on seven days were flown. For 1976 the F-4-C was at TIK 14 May through 17 June. Thunderstorm activity was below normal and only six flights, two of which were gust front investigations at 4-5,000 ft MSL, were flown. During these days, 45 of the penetrations had data sets which were sufficiently complete to be analyzed.

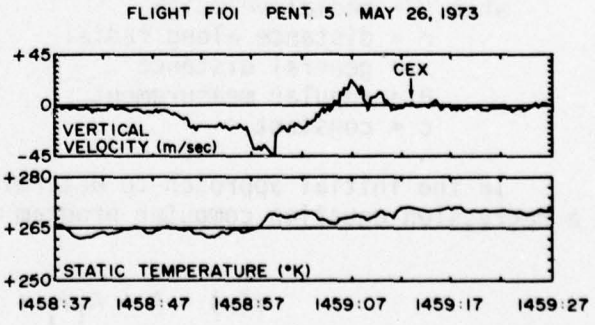

Figure 3-4. Vertical wind velocities during the thunderstorm penetration 26 May 1973. (CEX = cloud exit.)

TABLE 4-1

F-4-C AIRCRAFT PENETRATION FLIGHTS

1974		1975		1976	
DATE	ALTITUDE	DATE	ALTITUDE	DATE	ALTITUDE
April 21	12 and 15,000 ft	May 22	10,000 ft	May 24	10,000 ft
April 28	15,000	May 24(2)	8,000	May 21	16,000
May 21	16,000	May 26	12,000	May 29	4 and 5,000
May 23	16,000	May 29	15,000	May 30	5,000
May 24	14,000	June 8(2)	20,000	June 12	20,000
May 25(2)	14,000	June 5	(no data)	June 17	15,000
May 31	13 and 15,000	May 19	(no data)		

4.2 Data Analysis

The following Doppler radar derived parameters were considered:

1. Radar reflectivity (Z)(dBZ).
2. Reflectivity gradients $\frac{\Delta z}{\Delta r}$, $\frac{\Delta z}{\Delta \theta}$, $\frac{dBZ}{km}$.
3. Mean radial velocity $(\bar{v})(m\ s^{-1})$.
4. Maximum velocity gradient (shear) $x = s^{-1}$.
5. Spectrum breadth of the mean velocity $B = m\ s^{-1}$.
6. Gradient of the gradient $\frac{\partial^2 f}{\partial x \partial y} = s^{-1}\ m^{-1}$.
7. Laplacian $\nabla^2 f = s^{-1}\ m^{-1}$.

when v = radial velocity
r = distance along radial
x = general distance
θ = angular measurement
c = constant.

In the initial approach to determining potential significant parameters, a regression equation computer program was developed in the form

$$f(x) = A + A_1Y_1 + A_2Y_2 \ldots + A_iY_i$$

where x = derived gust velocity (U_{de}); Y_1, Y_2 ... Y_i are independent variables such as reflectivity, mean wind, wind shear and A_1, A_2 ... A_i are weighted coefficients related to the correlation. Using the first two years of data, as input no single significant element was apparent. We thus considered the problem from a second viewpoint: if a parameter is to be a reliable indicator, then it must exceed a threshold value whenever turbulence above an assigned value is encountered. This led to a second computer program development which took the form: if $U_{de} \geq M$ then $Y_{i(max)} \geq A_i$. That is, whenever the derived gust velocity exceeds a critical value (M) then the indicator parameter (Y_i) equals or exceeds a set value (A_i).

This is depicted in time(space) cross-sections of the variables along the flight path. The details of the Doppler data processing program are given in Appendix A and the time-history concept in Appendix B.

4.3 Relation of Doppler Spectrum Broadness to Aircraft Turbulence

Figure 4-1 is a typical plot. Values of U_{de}, B, $\partial v/\partial x$, $\partial v/\partial x \partial y$, and $\nabla^2 v$ are plotted using the corresponding linear scales at the left. The

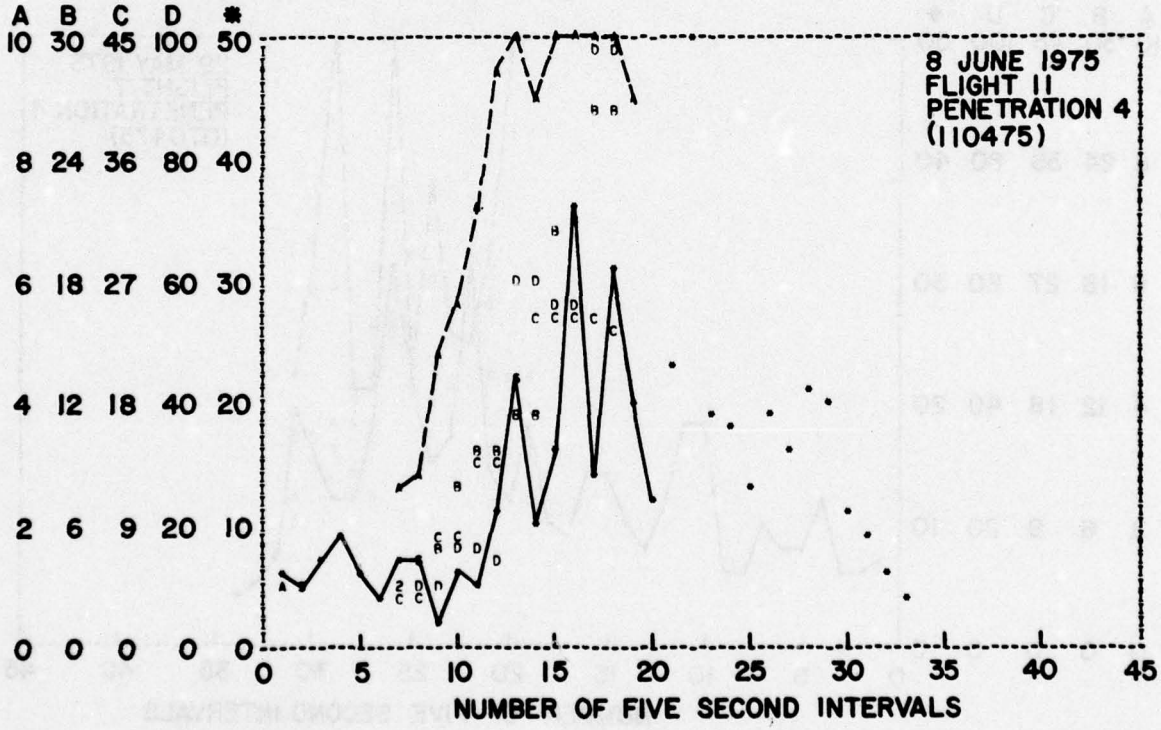

*Figure 4-1. 8 June 1975 penetration 4: Time (space) cross-section for maximum values recorded for each five seconds of flight or corresponding Doppler radar volume during penetration. Derived gust velocity = *(ft s^{-1}); spectrum breadth = A(m s^{-1}); velocity gradient = B (s^{-1} x 1000); gradient of the gradient = C(s^{-1} m^{-1} x 1000). Solid line connects values of spectrum breadth and dashed line, the derived gust velocities. D = Laplacian; 2 = two data points at the same place; 3 = three data points at the same place. $ is used when one or more "variables" are plotted at the same point as an observed derived gust velocity.*

scales were placed so that what was expected to be critical values were on the same horizontal line. Thus we have a B = 4 m s^{-1} on the same line as U_{de} = 6.1 m s^{-1} (20 ft s^{-1}) corresponding to moderate turbulence.

Note in this same figure how well the turbulence trend matches the trend in the width plot. Figure 4-2 and 4-3 are additional typical examples. Similar graphs were produced for all 45 cases. It is apparent if a $U_{de} \geq$ 6.1 m s^{-1} (20 ft s^{-1}) (moderate turbulence) value is considered as critical, that the spectrum broadness successfully flags these occurrences. The statistic probabilty of detection (POD) is described by Donaldson et al. (1975) and is given by

$$POD = X \quad (X + Y)$$

where "X" is a successful "forecast"--and "Y" is a miss. We apply this test to a turbulence "forecast" using the number of encounters when $U_{de} \geq$ 6.1 m s^{-1} and B $\geq$ 4 m s^{-1} as X and number of occasions $U_{de} \geq$ 6.1 m s^{-1} and B < 4 m s^{-1} as Y.

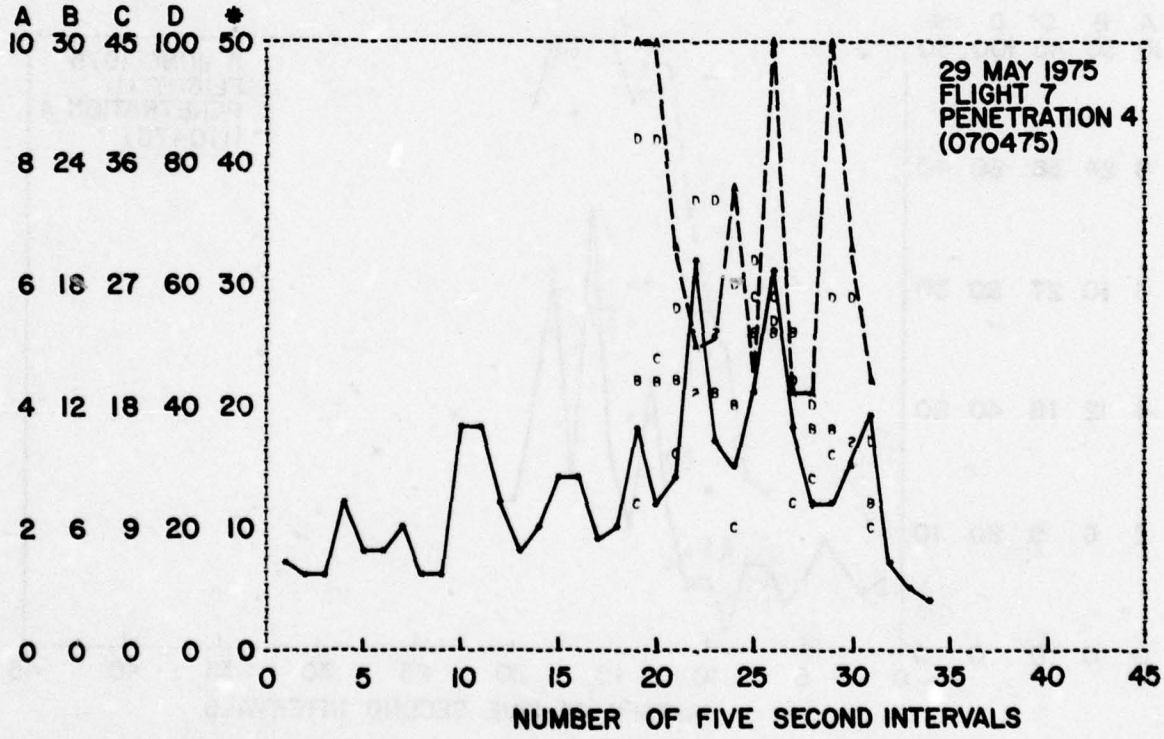

*Figure 4-2. 29 May 1975 penetration 4: Time (space) cross-section for maximum values recorded for each five seconds to flight or corresponding Doppler radar volume during penetration. Derived gust velocity = *(ft s^{-1}); spectrum breadth = A(m s^{-1}); velocity gradient = B (s^{-1} x 1000); gradient of the gradient = C(s^{-1} m^{-1} x 1000). Solid line connects values of spectrum breadth and dashed line, the derived gust velocities. D = Laplacian; 2 = two data points at the same place; 3 = three data points at the same place. $ is used when one or more "variables" are plotted at the same point as an observed derived gust velocity.*

Table 4-2 is a tabulation of the number of 5 second intervals during which $U_{de} \geq 6.1$ m s^{-1} (20 ft s^{-1}). The 76 occurrences during 45 penetrations had B values ≥ 4.0 within 1 km on 71 of these encounters, this yields a POD = 0.93. One of the missed cases had B ≥ 4.0 m s^{-1} within 2 km which would raise the POD to 0.95. In analyzing two additional cases it appears from the recorded aircraft elevator deflection that the U_{de} values may be contaminated by pilot input but the amount of contamination has not been determined.

Doviak et al. (1976) have calculated the cumulative probability of spectrum broadness within the entire storm for two tornadic storms (Fig. 4-4). Note that for B ≥ 4 m s^{-1} this probability is only about 30%. For non-severe storms the probability should be even less.

It is recognized that the second moment reflects not only turbulence but also wind shear and beam broadening. These have been discussed by

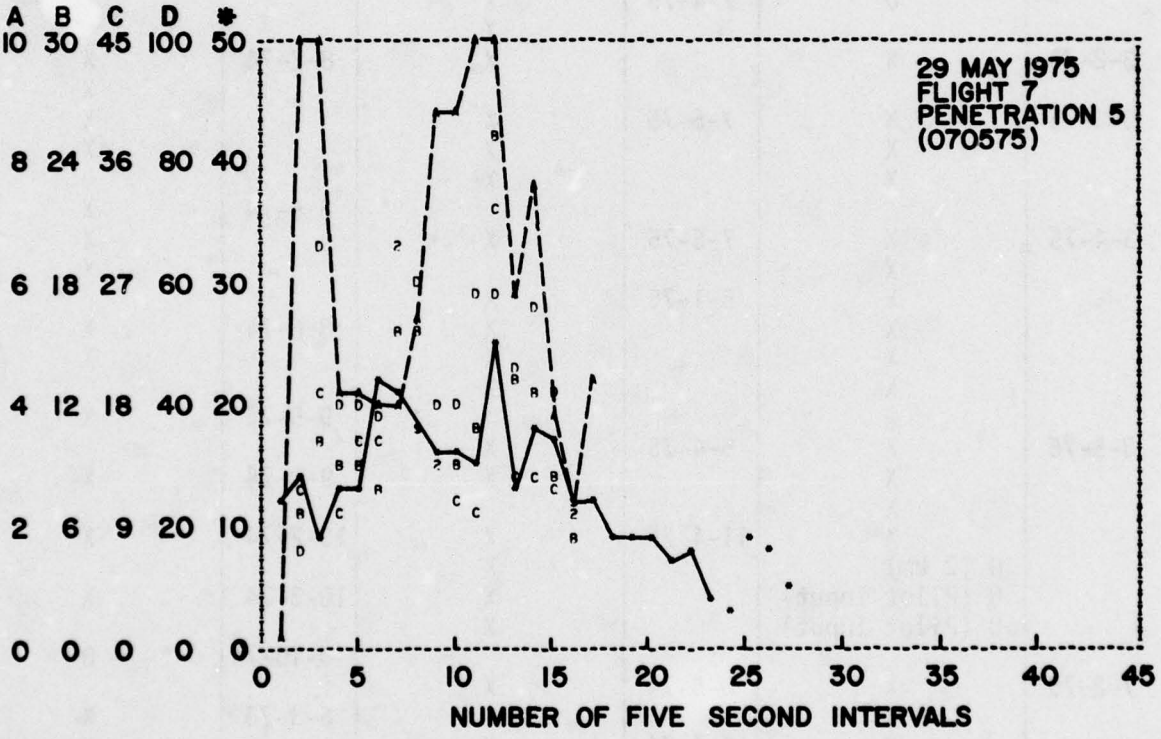

*Figure 4-3. 29 May 1975 penetration 5: Time (space) cross-section for maximum values recorded for each five seconds to flight or corresponding Doppler radar volume during penetration. Derived gust velocity = *(ft s^{-1}); spectrum breadth = A(m s^{-1}); velocity gradient = B (s-1 x 1000); gradient of the gradient = C(s^{-1} m^{-1} x 1000). Solid line connects values of spectrum breadth and dashed line, the derived gust velocities. D = Laplacian; 2 = two data points at the same place; 3 = three data points at the same place. $ is used when one or more "variables" are plotted at the same point as an observed derived gust velocity.*

TABLE 4-2

A. Occurrences of all Derived Gust Velocities 6.1 m s^{-1} (20 ft s^{-1}) and Concurrent Spectrum Broadness Values.

X = B ≥ 4 (during interval); X = B ≥ 4 within 1 km;
O = B < 4 m s^{-1} N.P. = no U_{de} ≥ 6.1 m s^{-1} during run.

Flight Ident.	B when U_{de} ≥ 6.1 m s^{-1}	Flight Ident.	B when U_{de} ≥ 6.1 m s^{-1}	Flight Ident.	B when U_{de} ≥ 6.1 m s^{-1}
3-1-75	X	7-3-75	X	7-1-74	X
	X		X		X
	X		X		
	X		X	7-5-74	X
	X		X		
	X			8-1-74	X
	O	7-4-75	X		X
			X		
3-2-75	X		X	8-2-74	X
					X
3-3-75	X	7-5-75	X		X
	X		X		X
	X		X		
				8-5-74	X
3-4-75	X	7-6-75	X		X
	X				X
	X	5-1-75	X		
	X		X	8-6-74	X
	X		X		X
	X		X		
				9-5-74	X
3-5-75	X	5-4-75	X		
	X		X	9-9-74	X
	X				
	X	11-4-75	X	10-2-74	X
	O (2 km)		X		
	O (Pilot Input)		X	10-3-74	X
	O (Pilot Input)		X		
				10-10-74	O
7-2-75	X	6-5-74	X		
	X			6-3-75	X
	X	6-4-74	X		X
	X		X		
	X		X		

B. Penetrations which did not Encounter U_{de} ≥ 6.1 m s^{-1}

3-2-74	9-6-74	10-11-74	10-2-75
6-2-74	10-4-74	3-4-75	10-3-75
6-6-74	10-5-74	4-4-75	10-4-75
7-6-74	10-6-74	4-5-75	11-3-75
9-1-74	10-8-74	5-6-75	

Sirmans and Doviak (1973) in detail. This does mean that there will be areas of high B which will not be turbulent. However since these areas comprise only a small portion of a storm an "overforecast" appears to be acceptable.

The other parameters investigated were not as successful and when quantities involving shear alone are used, the dependence on viewing angle (tangential shear cannot be determined) would appear to reduce the operational effectiveness. Turbulence due to convective processes appears to be isotropic (Houbolt, et al., 1964) (Ashburn et al., 1970) and therefore the spectrum width is less dependent on viewing angle.

We tried to address the question of high standard deviation locations within a storm. Insufficient Doppler data are available for any conclusion to be final. However Figure 4-5 and 4-6 are presented to show probable correlations between turbulence and the up- (down) drafts. These figures are derived from a study by Ray (1975) of tornadic storms. He uses the equation of continuity and dual-Doppler winds to calculate the 3-dimensional storm structure. We show here only a 5 km height section for which we analyzed the data. Note that the reflectivity maximum is north of the updrafts (positive). It is also apparent that the areas of large spectrum broadness are on the edges of the updraft with a preference for higher values when a downdraft is in close proximity. This suggests that the turbulence is produced by the shear (in the horizontal) of the vertical wind ($\Delta w/\Delta x$ or $\Delta w/\Delta s$) and that as more advances are made in thunderstorm understanding our ability to locate these areas will be improved. In addition vortex motion may also be turbulent.

4.4 Summary

The spectrum broadness of the radial velocity as observed by Doppler radar appears to be a useful indicator of thunderstorm turbulence. A POD = 0.95 is obtained for $B \geq 4.0$ m s^{-1}. These spectrum width estimates were equaled or exceeded in only slightly more than 30% of the volume within two

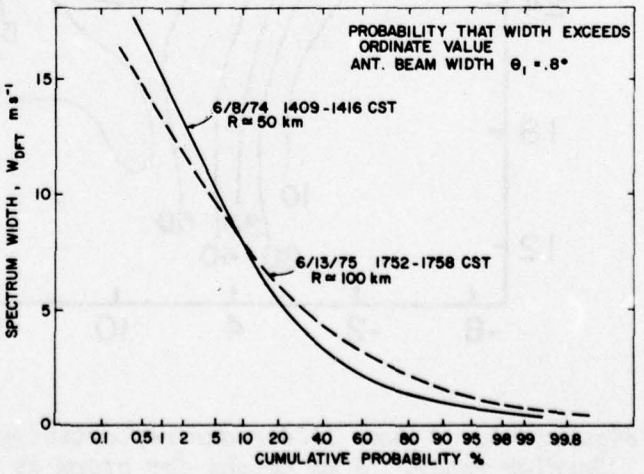

Figure 4-4. Cumulative probability of unbiased spectrum widths, W_{DFT}, for echoes from two tornadic storms.

tornadic storms and are seen less frequently in less severe storms. These turbulent areas are considered to be produced by differential shear in the vertical wind.

5. MESO-CYCLONIC AND TORNADO SIGNATURES

5.1 General

In addition to turbulence zones associated with vertical motion in thunderstorm areas containing organized vortices are also potentially hazardous to aircraft.

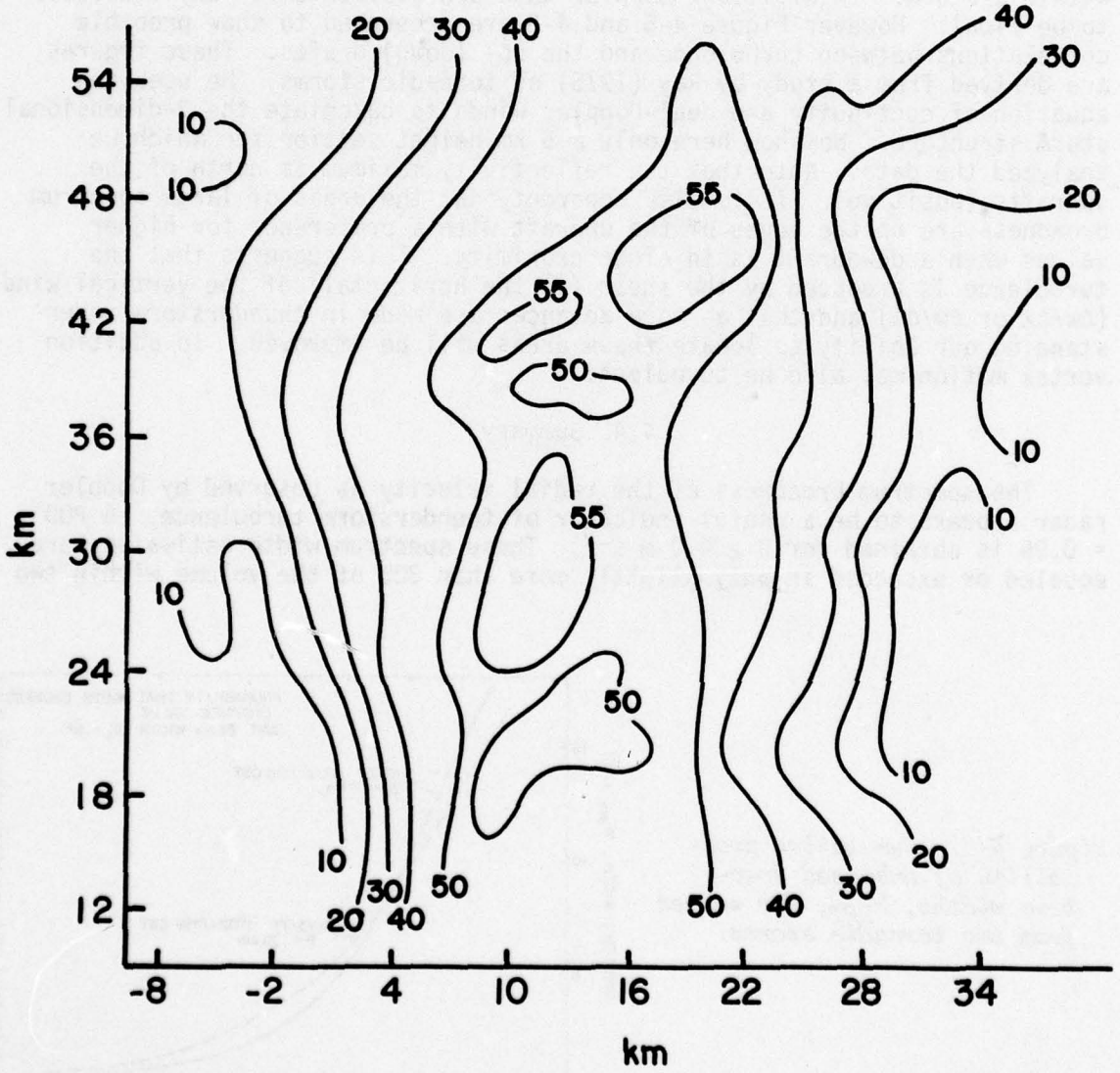

Figure 4-5. 8 June 1974 radar reflectivity contours (in dBz) from Norman Doppler radar. 5 km height for storm at Stillwater, Oklahoma.

Burgess (1976) and Brown and Lemon (1976) in work partially supported under this contract developed mesocyclone and tornado vortex signature recognition criteria applicable to single Doppler radar observations. As mentioned in Section 4, a single Doppler radar measures only the radial component of motion and is "blind" to motions perpendicular to the beam. Thus, unique "signatures" are desirable in identifying vortex motion when dual-Doppler systems are not practical or available.

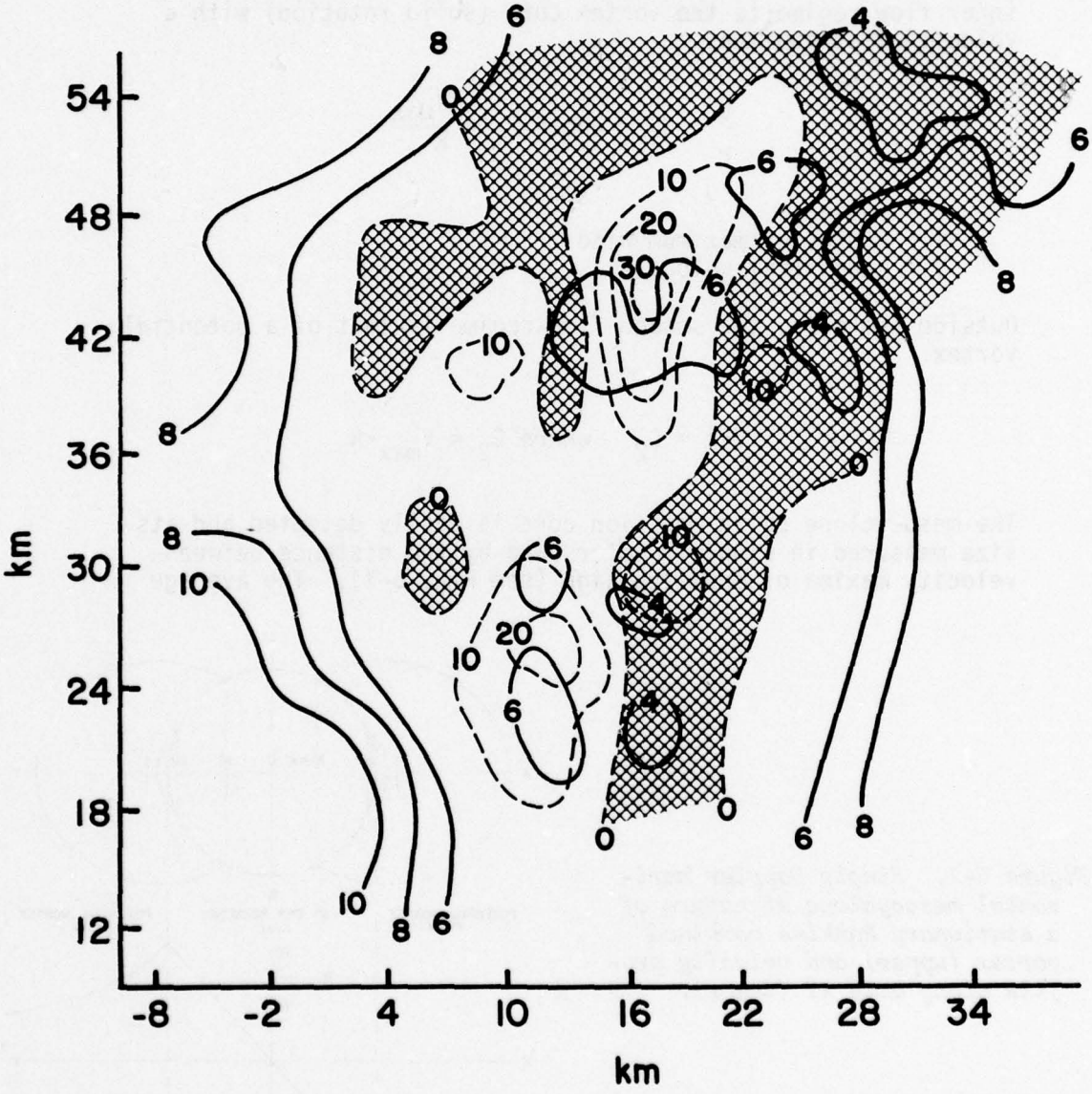

Figure 4-6. 8 June 1974: Spectrum breadth (m s^{-1}) contours are solid lines; vertical motion (m s^{-1}) contours are dashed lines. "+" is upward. Cross hatched area is downdraft.

5.2 Mesocyclone Signature

The mesocyclone circulation identification has been summarized by Burgess (1976) as follows:

> If a single Doppler radar were to scan a stationary non-divergent mesocyclone circulation having the tangential velocity distribution (two flow regimes) of a Rankine combined vortex, a characteristic velocity pattern would result (Fig. 5-1). The inner flow regime is the vortex core (solid rotation) with a velocity distribution:
>
> $$\frac{V}{r} = C_1 \quad \text{where } C_1 = \frac{V_{max}}{R}$$
>
> r = radius
> R = radius of maximum wind
> V = tangential velocity
>
> Outside the core, the second flow regime is that of a potential vortex:
>
> $$V \cdot r = C_2 \quad \text{where } C_2 = V_{max} \cdot R$$
>
> The mesocyclone solid rotation core is easily detected and its size measured in single Doppler data by the distance between velocity maxima of opposite sign (see Fig. 5-1). The average

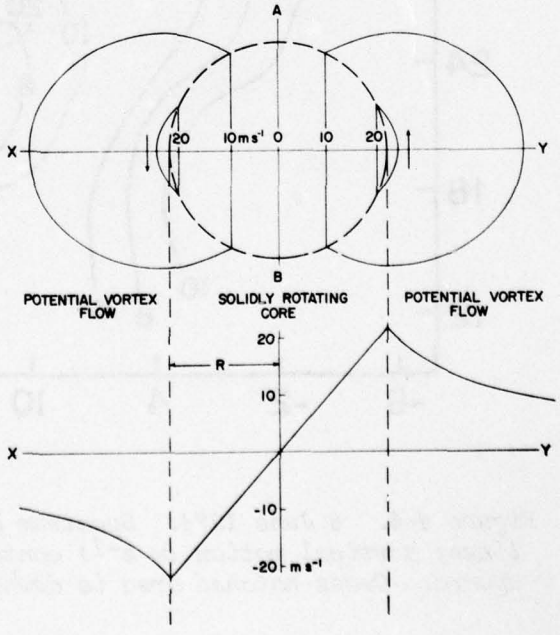

Figure 5-1. Single Doppler horizontal mesocyclone signature of a stationary Rankine combined vortex (upper) and velocity profile along axis XY (lower).

core diameter of NSSL data is 5.7 km with diameters being larger during early mesocyclone life and shrinking during tornado production. The outer potential vortex region is difficult to detect in single Doppler data but NSSL dual-Doppler data suggest its circulation region is about twice the core size. All measurements for the mesocyclone used in this paper pertain only to core diameter and not to potential vortex diameter.

The characteristic velocity pattern or couplet results because tangential flow perpendicular to the radar beam produces zero velocity along a radial line from the radar through the center of circulation. Closed velocity contours (isodops) appear at the radius of maximum wind where the radar beam is parallel to the tangential flow. The presence of convergence (divergence) rotates or skews the pattern clockwise (counterclockwise) relative to the radial line from the radar to the circulation center. Single Doppler mesocyclone signatures in tornadic storms (Fig. 5-2) conform well with the idealized model and at most times are recognizable at first glance. Signature vertical continuity is achieved throughout the storm's lowest 8 to 10 kilometers. The signature has been verified as a closed cyclonic circulation several times, beginning with Brown et al. (1975). For the same storm, Ray et al. (1975) calculated the mesocyclone signature region to be coincident with high-speed updraft.

5.3 Mesocyclone Statistics

Table 5-1 is a list of the 37 mesocyclones which have been confirmed by satisfying the criteria previously mentioned. Three signatures from the original data set had to be eliminated because the data collection mode failed to establish their persistence. The 37 mesocyclonic storms are a subset of the approximately 350 storms scanned by single Doppler from Spring 1971 to Spring 1975. At least 23 mesocyclones (62%) are associated with reported tornadoes. Storm Data (1971-1975) was used as the tornado report

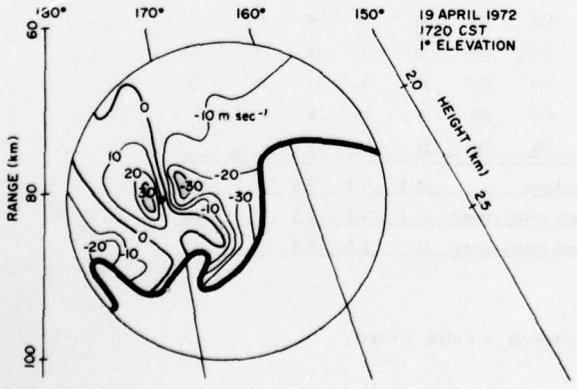

Figure 5-2. Single Doppler velocity field with mesocyclone signature at the time of a tornado (black dot).

Table 5-1. Mesocyclone Statistics.

Date	Beginning Time (CST)	Beginning Range (km)	Beginning Azimuth (deg)	Ending Time (CST)	Ending Range (km)	Ending Azimuth (deg)	Rotational Velocity ($m\ s^{-1}$)	Horizontal Diameter (km)	Vertical Extent (km)	Severe Weather[A]	Lead Time (min)
June 2, 1971	2020[1]	88	333	2200[2]	13	340	20	5	NA	WH	-
April 19, 1972	1500[1]	152	315	1550[2]	133	328	20	9	7	TH	-
April 19, 1972	1655[1]	82	184	1745[2]	80	157	32	5	8	T*WH	-
April 19, 1972	1655[1]	90	186	1745[2]	88	153	20	5	8	TWH	-
May 22, 1972	2000[1]	148	272	2040	130	275	16	7	8	TH	23
May 22, 1972	2155[1]	165	260	2210[2]	162	262	13	5	5	TH	-
April 20, 1973	0025[1]	90	116	0040[2]	100	110	15	10	5	TW	-
May 24, 1973	1455	76	285	1610	40	290	20	2	9	T*H	37
June 4, 1973	1655	85	330	1750	60	350	23	11	8	H	-
June 4, 1973	1835[1]	38	320	1855[2]	25	355	20	7	8	TWH	NA
June 4, 1973	1855[1]	20	265	1940[2]	20	040	17	5	5	TWH	13
June 4, 1973	2020	47	203	2135	55	160	21	6	7	TWH	35
June 4, 1973	2105[1]	80	205	2215[2]	85	165	25	8	9	TWH[N]	-
June 4, 1973	2140[1]	105	190	2215[2]	105	180	18	8	9	T	41
June 18, 1973	1545	95	275	1645[2]	94	267	42	10	11	T*WH	58
April 20, 1974	1425[1]	90	255	1445	75	260	20	6	5	H	-
April 20, 1974	1430	65	260	1645	70	045	28	5	5	TH	26
May 22, 1974	2055[1]	80	355	2150	50	025	20	8	10	WH	-
May 23, 1974	1600	110	340	1740	50	040	22	6	8	H	-
May 23, 1974	1750[1]	60	315	1930	25	080	19	6	9	TWH	40
May 25, 1974	1325[1]	55	180	1425	80	145	20	5	5	WH	-
June 6, 1974	1530	60	270	1640	40	230	25	3	8	T(?)WH*	51
June 6, 1974	1612	70	232	1705	50	205	25	3	6	W	-
June 6, 1974	1633[1]	82	220	1730	85	205	20	5	6	TWH[N]	-
June 8, 1974	1315	30	285	1455	80	030	25	4	8	TH	23
June 8, 1974	1500[1]	60	010	1535	025	80	20	5	NA	-	-
June 8, 1974	1515	12	350	1635	80	045	25	5	8	T	31
June 8, 1974	1555	25	020	1650[2]	80	050	25	6	7	T	46
June 8, 1974	1630	15	045	1730[2]	80	052	25	4	7	T	51
June 8, 1974	1830[1]	20	085	1900[2]	45	055	25	4	NA	T	16
May 26, 1975	1530	95	150	1600[2]	110	150	15	4	7	H[N]	-
June 8, 1975	1540[1]	160	310	1700	140	320	20	5	NA	H	-
June 13, 1975	1400	95	012	1450[2]	115	020	20	5	8	H	-
June 13, 1975	1720[1]	106	017	1755	104	025	30	3	10	T*	13
June 13, 1975	1805	100	027	1930	095	052	32	5	11	TW	61
June 13, 1975	1805	95	015	1850	090	025	17	7	8	-	-
June 13, 1975	1825	90	012	1930	075	045	25	5	13	W	-
Average for all mesocyclones							22.3	5.7	7.8	-	-
Average for all tornadic mesocyclones							23.3	5.7	7.7	-	36
Average for maxi-tornado mesocyclones							31	5.0	9.5	-	41

[1] Mesocyclone well formed when data collection begun.

[2] Mesocyclone well formed when data collection ended.

[A] Source is Storm Data unless otherwise indicated: T = tornado, W = wind, H = hail.

[N] NSSL damage survey

* Maxi tornado

source (except for a few NSSL surveys) and a measurable percentage of tornadoes is not contained in storm data, particularly those occurring in rural areas after dark. Of the remaining 14 signatures, 12 are associated with damaging wind or hail. Fully 95% of all mesocyclones have produced some type of surface damage. At no time during data collection did a verified tornado occur unless preceded by a mesocyclone signature. The average lead time before tornado occurrence was 36 minutes. Some mesocyclones were well formed when data collection began and lead times could have been even longer.

The average mesocyclone has a rotational velocity of 22 m s^{-1}, a horizontal diameter of 5.7 km, and a vertical extent of 7.8 km. Very little difference in rotational velocity, horizontal diameter, or vertical extent is seen between tornadic and non-tornadic mesocyclones. However, mesocyclones which produce maxi-tornadoes have smaller horizontal diameters, are taller and rotate considerably faster.

5.4 Tornado Vortex Signatures

The tornado vortex is especially hazardous to aircraft and is much smaller than the mesoscale system of which it is a part. This poses additional recognition problems. Work on this phase has been reported by Brown and Lemon (1976) and excerpts follow:

When one considers the more typical (lower PRF) Doppler radar with limited velocity resolution, tornadic wind speeds will fold into the unambiguous velocity interval. The resulting broad spectrum fills the entire unambiguous interval, making it extremely difficult to unscramble the peak tornadic speeds. Using the 5.4 cm Air Force Cambridge Research Laboratories' Doppler radar, Kraus (1973) found filled spectra (12.5 m s^{-1}) in the vicinity of the Brookline, Massachusetts tornado of 9 August 1972. Zrnic et al. (1976) have estimated peak speeds by comparing numerical simulations with folded spectra measured by the 10 cm NSSL Doppler radar.

For low PRF data collection throughout a convective storm, the mean of the Doppler velocity spectrum is the parameter of primary interest. Up to the time of the NSSL Doppler velocity measurements in the Union City tornadic storm of 24 May 1973, the mean Doppler velocity field had not been expected to indicate the presence of a tornado. However, the data collected on that day did reveal a distinct tornadic vortex signature (TVS).

The single Doppler velocity signature of a vortex is a function of vortex size relative to radar beam size. Mesoscale vortices--having dimensions considerably greater than the beamwidth--produce a unique signature when mean Doppler velocity values are plotted as a function of range and azimuth (e.g., Donaldson, 1970; Burgess, 1976).

For vortices smaller than, but centered in, the radar beam, previously cited literature suggests that the single Doppler velocity signature of a tornado vortex should be a broad velocity spectrum with a mean of zero. However, when the radar beam is not centered on the vortex, it is difficult to accurately predict the spectra and mean Doppler velocity fields. Fortunately, Zrnic recently developed a model that simulates a Doppler radar looking at a Rankine combined vortex (see Zrnic and Doviak, 1975). The radar and vortex characteristics are completely flexible such that the model can be used to simulate Doppler velocity measurements in vortices ranging from very small tornadoes to large mesocyclones. The model also allows the reflectivity profile across the vortex to be varied.

The Zrnic model aids understanding of data from a finite Doppler radar beam scanning across a vortex. In a Rankine combined vortex (heavy curve in Fig. 5-3), the tangential velocity increases linearly until the maximum velocity at the outer edge of the "core" is reached then decreases inversely proportional to radius. Various sized vortices generated by the model can be normalized by dividing all velocities by the maximum core velocity and by dividing all lengths by the core radius. A uniform reflectivity profile is used for the simulations presented in this paper.

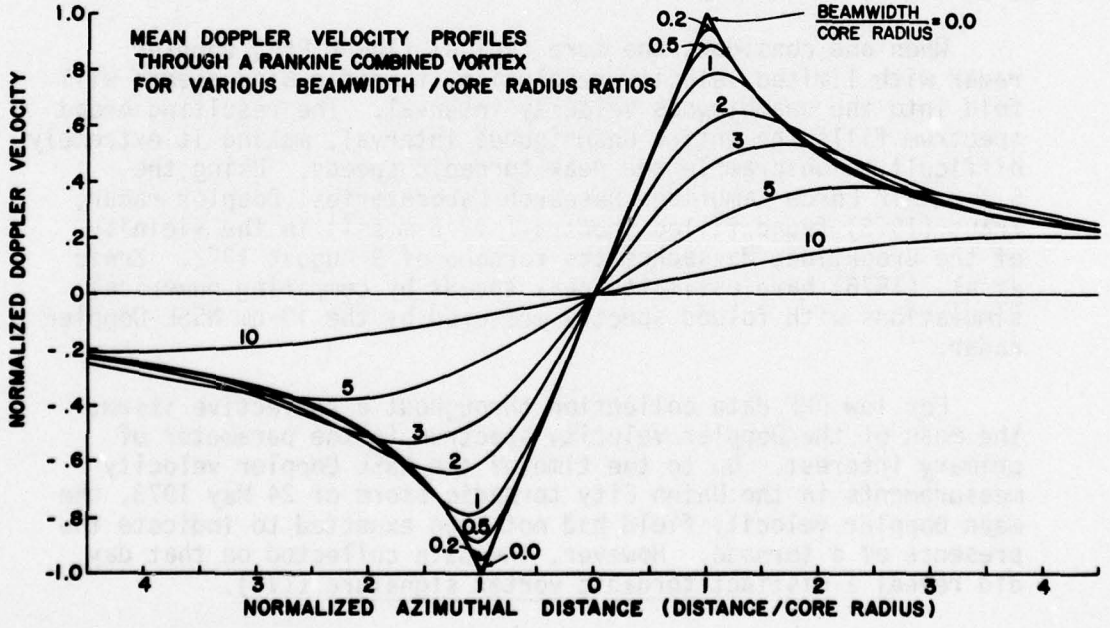

Figure 5-3. Theoretical change of mean Doppler velocity azimuthal profile through a Rankine combined vortex (heavy line labeled 0.0) as the beamwidth becomes progressively larger relative to the vortex core radius. Velocities and distances are normalized relative to peak vortex tangential velocity and core radius of peak velocity, respectively.

As indicated in Figure 5-3, when the radar half-power beamwidth is a small fraction of the vortex core radius (beamwidth/core radius ratios much less than one), the Doppler velocity measurements reproduce the mesoscale vortex very well. However, when the beam becomes significantly wider than the core radius, some portion of both the positive and negative vortex peaks will be within the beam unless the beam is entirely to one side of the vortex center. Therefore, one would not expect the mean Doppler velocity value to maximize until the beam has just cleared the vortex center. For example, when the beamwidth is three times the core radius, the peak is approximately 1.5 core radii or one-half beamwidth from the center. Likewise, for beamwidth 5 and 10 times greater than the core radius, the peaks are at approximately 2.5 and 5 core radii, respectively. Also, the wider the beam, the greater the smoothing of the true tangential velocity profile and consequently the smaller the magnitude of the peak Doppler velocities. Detectability decreases with range as the beam becomes wider relative to the vortex.

Since the Doppler velocity profiles appear to peak at a radius of about one-half beamwidth, the curves in Figure 1 were replotted relative to beamwidth. The resulting curves (Fig. 5-4) vividly protray what we call the tornadic vortex signature (TVS). The peak-to-peak diameter is not significantly affected by the size of the within-beam tornado. However, the signature amplitude, which is affected, plays an important role in TVS detectability. The TVS cannot be resolved unless the peak-to-peak Doppler velocity shear is appreciably greater than the background cyclonic shear produced by the parent mesocyclone.

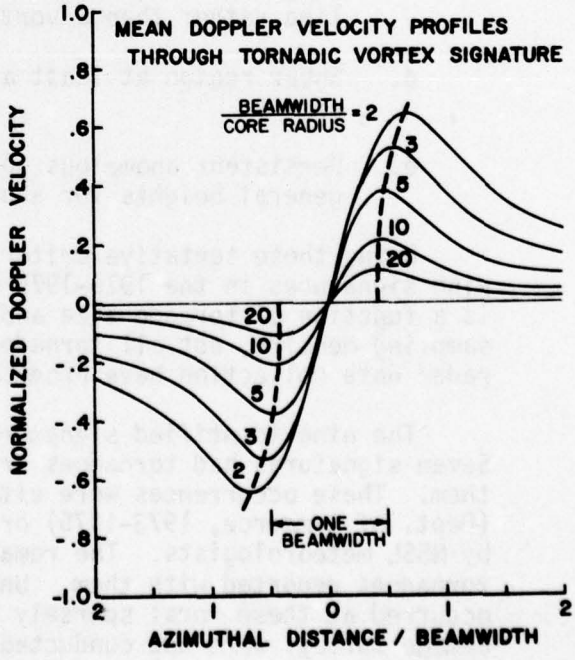

Figure 5-4. Theoretical change in size and magnitude of tornadic vortex signature (TVS) as radar beamwidth changes relative to core radius of peak tangential velocity in tornado.

Several other practical limitations must be considered when attempting to identify tornadic vortex signatures from mean Doppler velocity measurements. First of all, when data are collected at discrete azimuthal increments, peak values may not be sampled when the sampling interval is greater than one beamwidth. Secondly, Zrnic and Doviak (1976) have shown that a radar antenna rotating rapidly relative to the sampling time has an effectively broadened beamwidth. Thus, for a given peak tangential velocity and tornado size, the amplitude of the TVS will decrease as the antenna rotation rate increases.

5.5 Tornado Vortex Signature Statistics

Objective criteria for defining a tornadic vortex signature have not yet been established. We are in the process of analyzing all signatures and possible signatures found to data. A more thorough search of the NSSL Doppler radar archives also is underray. We do, however, have some tentative guidelines for defining a TVS. These guidelines are:

a. An azimuthal shear of at least 15 to 20 m s^{-1} over an azimuthal distance of 1 deg or less (1.25 beamwidths or less).

b. Signature cyclonic (TVS translation removed) with peak Doppler velocity values of opposite sign. (A rare anticyclonic TVS would not be excluded, however.)

c. Anomalous shear region not more than about 1 km range extent (otherwise it would indicate a shear line rather than a vortex).

d. Shear region at least a few kilometers in vertical extent.

e. Persistent anomalous shear region at the same general heights for about 10 min or more.

Using these tentative criteria, we thus far have identified nine signatures in the 1973-1975 data set. Since TVS detection is a function of tornado size and strength as well as radar sampling density, not all tornadoes in existence during Doppler radar data collection have produced noticeable signatures.

The nine identified signatures are listed in Table 5-2. Seven signatures had tornadoes or funnel clouds associated with them. These occurrences were either documented from Storm Data (Dept. of Commerce, 1973-1975) or from damage surveys conducted by NSSL meteorologists. The remaining two signatures had no tornadoes reported with them. Unfortunately, we do not know what occurred at these rural sparsely populated locations because damage surveys were not conducted.

5.6 Summary

Mesocyclones associated with thunderstorms and tornadoes can be identified from single Doppler mean velocity fields by applying objective criteria to regions of cyclonic shear.

The presence of a tornado vortex within a Doppler radar sampling volume also results in a unique signature but it is not as easily identified. Both signatures however do provide a means for identifying these circulations which are also hazardous to aircraft operations.

6. GENERAL SUMMARY AND CONCLUSIONS

The spectrum broadness of the radial velocity as observed by Doppler radar appears to have a high potential as an indicator of thunderstorm turbulence. In the 76 turbulence encounters having $U_{de} \geq 6.1$ m s^{-1} (20 ft s^{-1}) the turbulent regions were associated with Doppler radar radial velocity "B" values ≥ 4 m s^{-1} within 2 km 72 times for a POD = 95%. In addition thunderstorm associated mesocyclones and tornadoes hazardous to aircraft operation can be identified using single Doppler velocity fields by applying objective criteria.

Utilization of these parameters in the air space system is dependent on information availability and accessibility. Toward this end the occtant change counter method of estimating mean velocities was developed. Further development led to the multi-moment display which now provides on a single display in real time the reflectivity, mean velocity, and spectrum broadness at grid locations within a storm. Thus the goal of increased safety and better utilization of air space in thunderstorm conditions appears attainable.

TABLE 5-2

TORNADIC VORTEX SIGNATURES AND ASSOCIATED WEATHER PHENOMENA

Date	Location	Associated Phenomena
24 May 1973	Union City, OK	Tornado, Hail
23 May 1974	Yukon, OK	Tornado
6 June 1974	Tabler, OK	?
8 June 1974	Oklahoma City, OK	Tornado
8 June 1974	Harrah, OK	Tornado
13 June 1975	Stillwater, OK	Tornado
13 June 1975	Ripley, OK	Funnel Aloft
13 June 1975	Cushing, OK	Funnel Aloft
13 June 1975	Kendrick, OK	?

7. RECOMMENDATIONS

Continued refinement of the models and development for the use of Doppler radar should be continued. Further development of the real time displays and automation needs to be supported. Means for using Doppler radar effectively in the National Air-Space system should be developed because this probe has great promise for mitigating thunderstorm associated flight hazards.

8. ACKNOWLEDGMENTS

Mr. Thomas Jobson's and Mr. Phillip Bothwell's assistance in developing the computer programs and in combining the aircraft flight path with the Doppler radar presentations is greatly appreciated. All NSSL staff contributed to the success of this multi-observational program and their contributions are recognized.

REFERENCES

Armstrong, G. and R. Donaldson, Jr., 1969: Plan shear indicator for real-time Doppler radar identification of hazardous storm winds. J. Appl. Meteor., 8, 376-383.

Ashburn, E. V., D. E. Waco and C. A. Melvin, 1970: High altitude gust criteria for aircraft design. Air Force Flight Dynamics Laboratory Technical Report AFFDL-TR-70-101, October 1970, 68 pp.

Berger, T., and H. L. Groginsky, 1973: Estimation of the spectral moments of pulse trains. Presented at Intern. Conf. Information Theory, Tel Aviv, Israel.

Brown, R. A. and L. R. Lemon, 1976: Single Doppler radar vortex recognition: Part II--Tornadic Vortex Signature. Preprint 17th Conf. on Radar Meteor., Oct. 26-29, 1976, Seattle, Am. Meteor. Soc., 104-109.

_____, D. W. Burgess, J. K. Carter, L. R. Lemon and D. Sirmans, 1975: NSSL dual-Doppler radar measurements in tornadic storms: A preview. Bull. Amer. Meteor. Soc., 56, 524-526.

_____, W. C. Bumgarner, K. C. Crawford and D. Sirmans, 1971: Preliminary Doppler velocity measurements in a developing radar hook echo. Bull. Amer. Meteor. Soc., 52, 1186-1188.

Burnham, J. and J. T. Lee, 1969: Thunderstorm turbulence and its relationship to weather radar echoes. J. of Aircraft, 6, 5, 438-445.

Burgess, D. W., 1976: Single Doppler radar vortex recognition: Part I--mesocyclone signatures. Preprints, 17th Conf. on Radar Meteor., Oct. 26-29, Seattle, Am. Meteor. Soc., Boston, 97-103.

_____, L. Hennington, R. J. Doviak and P. S. Ray, 1976: Multimoment Doppler display for severe storm identification. J. Appl. Meteor., 15, 12, 1302-1306.

Donaldson, R. J., Jr., R. M. Dyer and M. J. Kraus, 1975: An objective evaluator of techniques for predicting severe weather events. Proc. Ninth Conf. on Severe Local Storms, Am. Meteor. Soc., Boston, Mass., 321-326.

_____, 1970: Vortex signature recognition by a single Doppler radar. J. Appl. Meteor., 9, 661-670.

Doviak, R. J., D. Sirmans and D. Zrnic, 1976: Resolution of pulse-Doppler radar range and velocity ambiguities in severe storms. Preprints, 17th Conf. on Radar Meteor., Oct. 26-29, Seattle, Am. Meteor. Soc., Boston, 15-22.

_____ and D. Sirmans, 1973: Doppler radar with polarization diversity. J. Atmos. Sci., 30, 4, 737-738.

Houbolt, J. C., R. Steiner and K. Pratt, 1964: Dynamic response of airplanes to atmsopheric turbulence including flight data or input and response. NASA Technical Report TR R-199 NASA Washington, D.C., June 1964, 7-18.

Kraus, M. J., 1973: Doppler radar observations of the Brookline, Massachusetts tornado of 9 August 1972. Bull. Amer. Meteor. Soc, 54, 519-524.

Lee, J. T. and M. Kraus, 1975: Plan shear indicator and aircraft measurements of thunderstorm turbulence: Experimental results. Preprints, 16th Radar Conf., Apr. 22-24, Houston, Tx., Am. Meteor. Soc., 337-340.

Ray, P. S., R. J. Doviak, G. B. Walker, D. Sirmans, J. Carter and B. Bumgarner, 1975: Dual-Doppler observation of a tornadic storm. J. Appl. Meteor., 14, 1521-1530.

Ryan, J., A. Berens, A. Robertson, R. Dominic, K. Rolle, 1971: Medium altitude critical atmospheric turbulence (MEDCAT). Data Processing and Analysis, AF Technical Report AFFDL-TR-71-82. Air Force Systems Command, July, 602 pp.

Sirmans, D., 1973: Real-time estimate of mean velocity by averaging quantized phase displacements of Doppler radar echoes. 1973 SWIEEECO Record of Technical Papers. 25th Annual Southwestern IEEE Conference, 71-72.

_____, and R. J. Doviak, 1973: Meteorological radar signal intensity estimation. NOAA Tech. Memo ERL NSSL-64, 80 pp.

Zrnic, D. S. and R. J. Doviak, 1975: Velocity spectra of vortices scanned with a pulse-Doppler radar. J. Appl. Meteor., 14, 1531-1539.

_____ and _____, 1976: Effective antenna pattern of scanning radars. IEEE Transactions on Aerospace and Electronic Systems, AES-12, 5, 551-555.

_____, _____, D. Burgess and D. Sirmans, 1976: Tornado characteristics revealed by a pulse-Doppler radar. Preprints, 17th Conf. on Radar Meteor., Boston, Amer. Meteor. Soc.

APPENDIX A

Doppler Radar Data Processing Program--PPI-scan

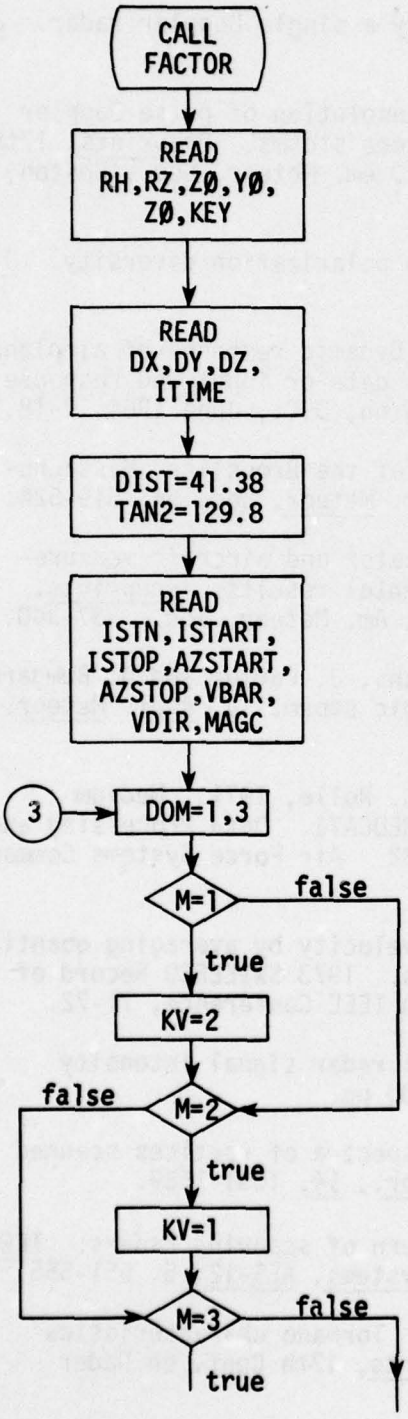

FACTOR - library subroutine--controls size of all plots by its argument.

RH - horizontal radius of influence KM
RZ - vertical radius of influence KM
XØ,YØ - SW corner of grid
ZØ - beginning elevation angle
KEY - determine variable to be fit--0-vel, 1-std, 2-Z, 3-all
DX,DY - horizontal grid increments KM
DZ - vertical grid increment deg
ITIME - reference time if horizontal motion used

DIST - straight line distance between NRO-CIM KM
TAN2 - angle NRO-CIM

ISTN - station number 1-NRO(D), 2-CIM(D), 3-NRO(57)
ISTART, ISTOP - starting and stopping times
AZSTART, AZSTOP - starting and stopping azimuth
VBAR, VDIR - horizontal motion
MAGC - AGC cutoff

loop disregarded if KEY ≠ 3

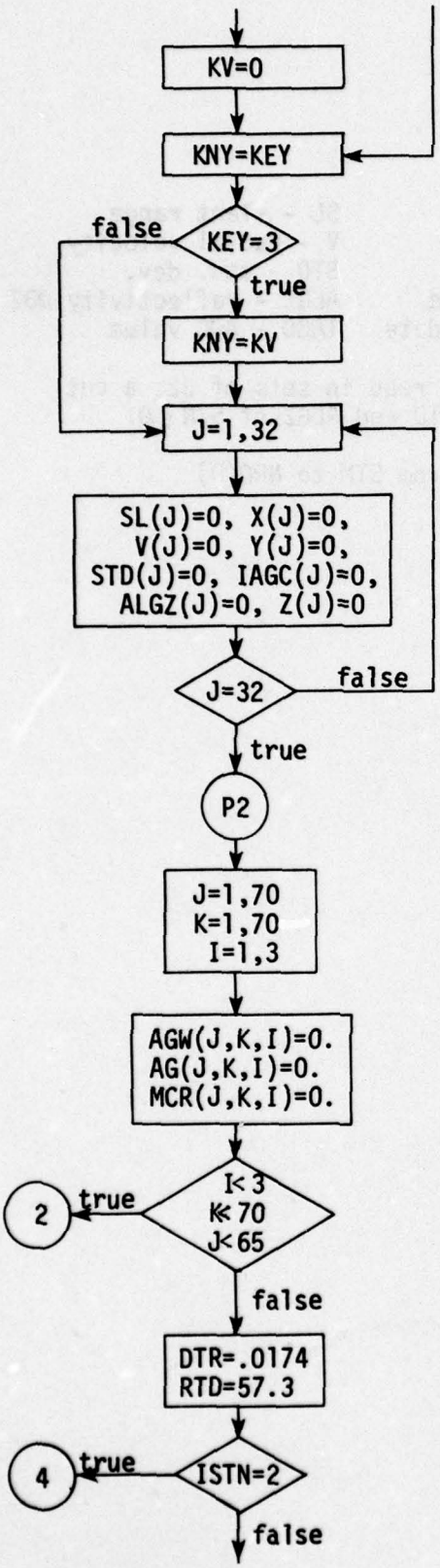

Setting KNY to variable to be fit
- 0 - vel
- 1 - std
- 2 - Z
- 3 - all 3

Initializing arrays
SL - slant range
V - velocity (radial)
STD - standard deviation of radial velocity
ALGZ - reflectivity dBZ
X,Y,Z - cartesian coordinate with respect to NRO 0° elevation plane
IAGC - power

AGW - Cressman dividend
AG - Cressman divisor
MCR - character array used to indicate # plts interpolated to each grid point

conversion degrees - radians

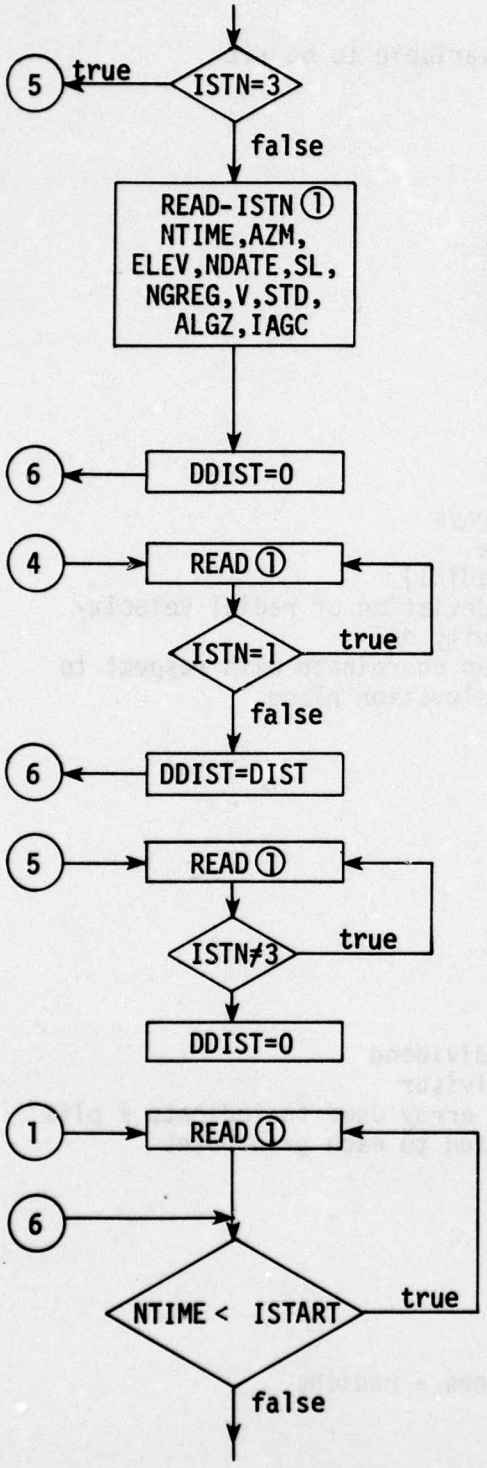

NTIME - time
AZM - azimuth
ELEV - elevation
NDATE - julian date
NGREG - gregorian date

SL - slant range
V - radial velocity
STD - std. dev.
ALGZ - reflectivity dBZ
IAGC - AGC value

SL,V,STD,ALGZ,IAGC read in sets of 32; a cut has been made on STD and ALGZ of $S/N \leq 0$.

DDIST = distance from STM to NRO(D)

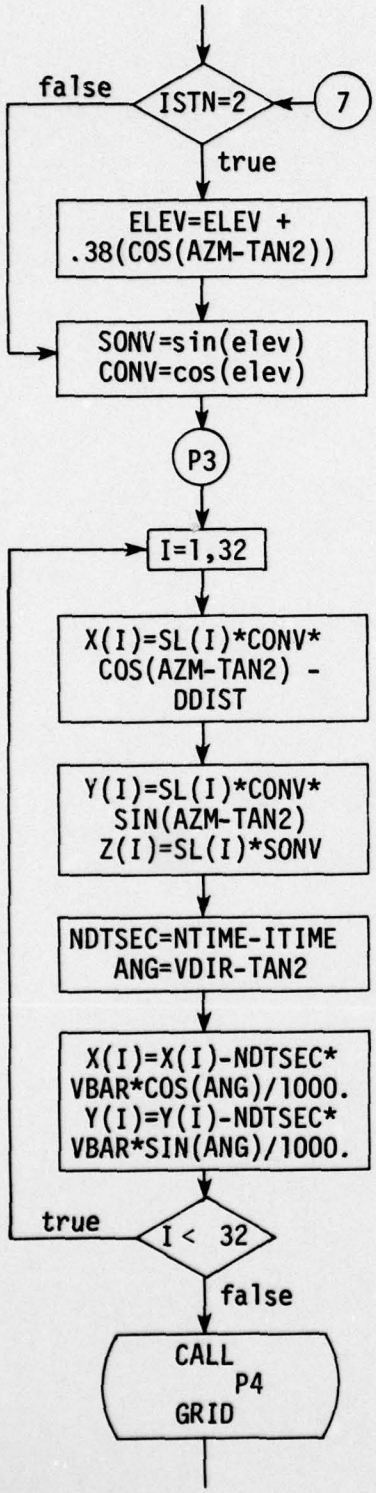

correct for either curvature on elevation

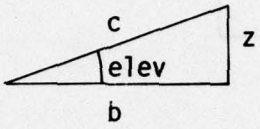

$$SONV = \frac{Z}{c}$$

$$CONV = \frac{b}{c}$$

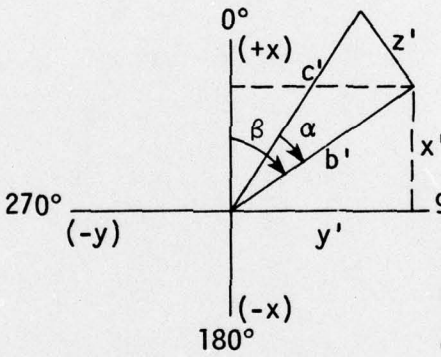

$SL(I) = c'$

$CONV = \frac{b'}{c'}$ $\quad SONV = \frac{z'}{c'}$

α = elev

β = AZM-TAN2

correct data pt. to a common time in space using storm motion.

$$X(I) = c' * \frac{b'}{c'} * \frac{x'}{b'} = x'$$

$$Y(I) = c' * \frac{b'}{c'} * \frac{y'}{b'} = y'$$

$$Z(I) = c' * \frac{Z'}{c'} = Z'$$

NDTSEC - difference in time (sec) between data pt. and reference time

ANG - wind direction w/R to coplane grid

Subroutine GRID places data pts. onto grid.

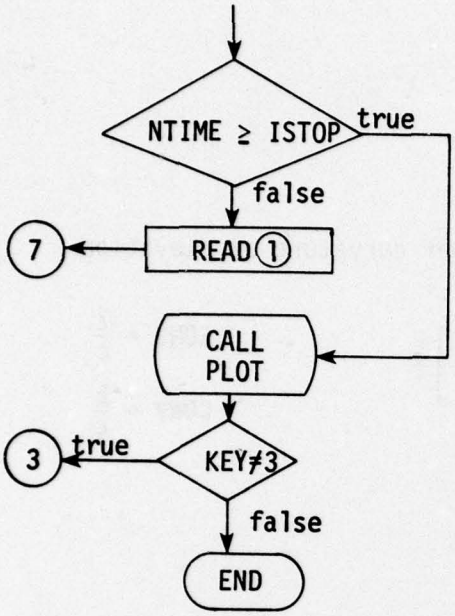
NTIME ≥ ISTOP
true
false
7
READ (1)
CALL
PLOT
3
true
KEY≠3
false
END

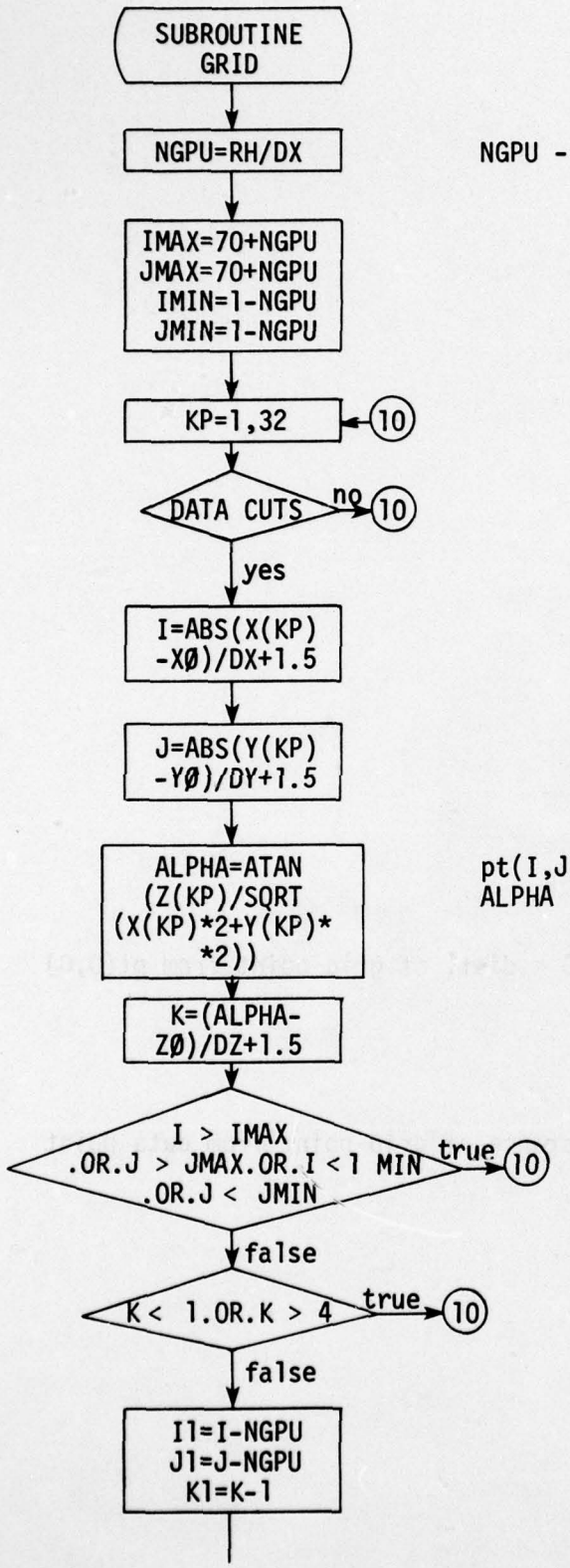

NGPU - number of grid points w/i radius of influence
i.e. RH = 1.5 DX = .5
NGPU = 1.5/.5 = 3

pt(I,J,K) - closest grid point to data pt.
ALPHA - elevation of data point from NRO(D)

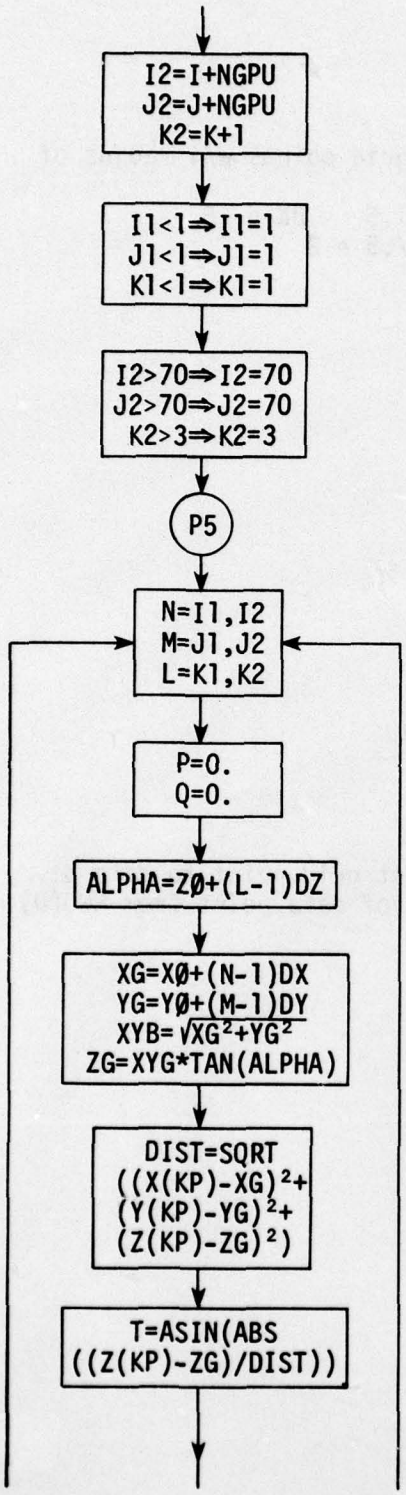

XG,YG,ZG = dist. of grid point from pt(0,0)

DIST=distance of grid point from data point

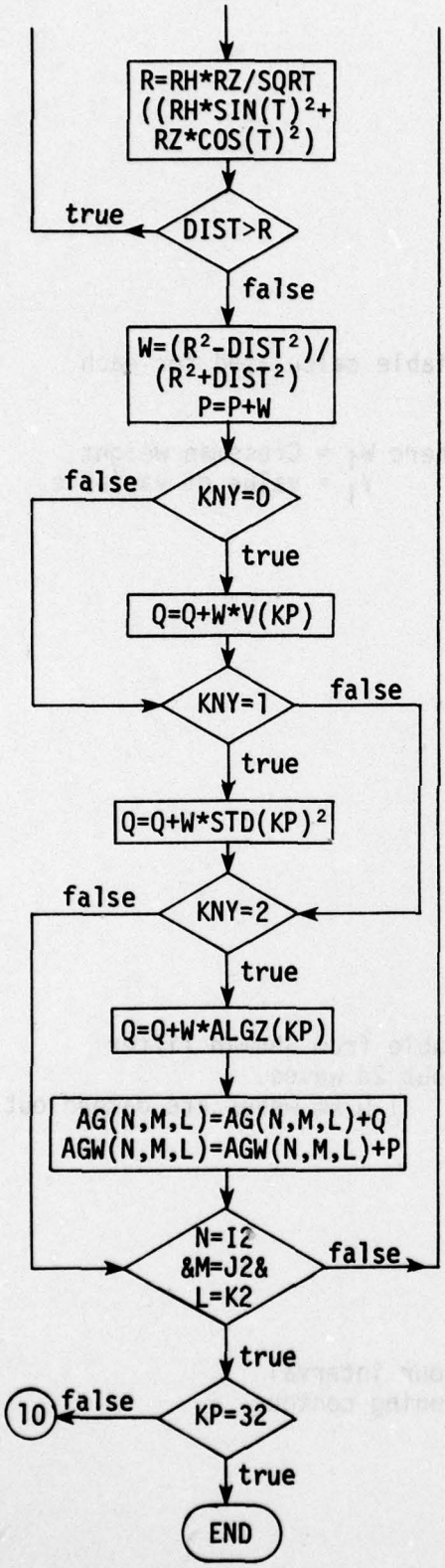

R - radius of influence

W - Cressman weight

$$Z = \frac{\Sigma W_i Z_i}{\Sigma W_i}$$ where Z = value of grid point

Z_i = value of data point

AG - Cressman numerator
AGW - Cressman denominator

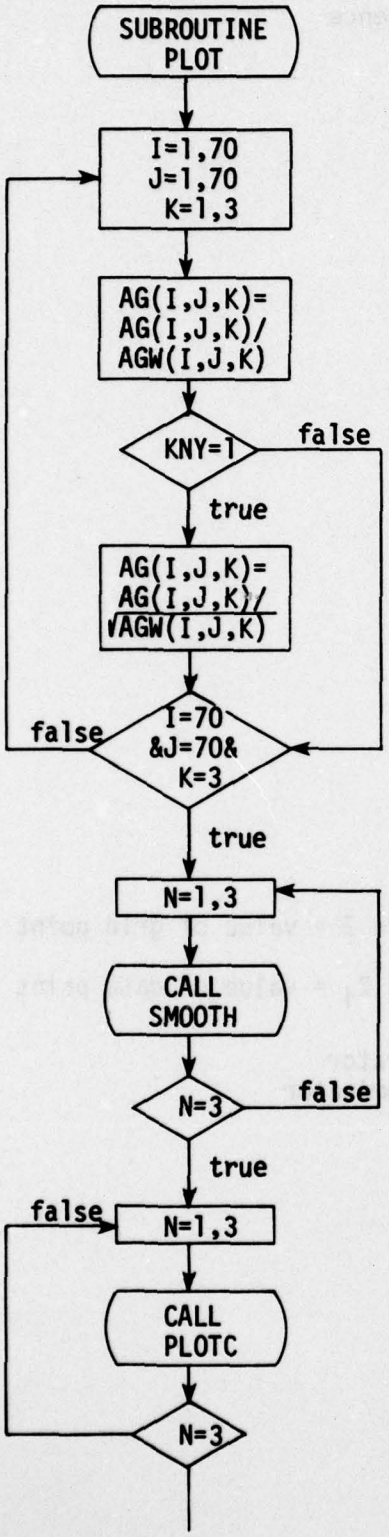

AG = value of variable calculated for each grid point

$$= \frac{\Sigma W_i V_i}{\Sigma W_i}$$ where W_i = Cressman weight, V_i = value of variable

6th argument variable from Shuman filter
= .25 damps out 2d waves.
i.e. DX = .5 1.0 km waves are damped out.

1st argument contour interval
2nd argument beginning contour

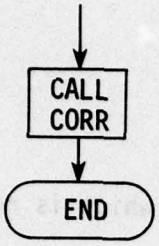
CALL
CORR
END

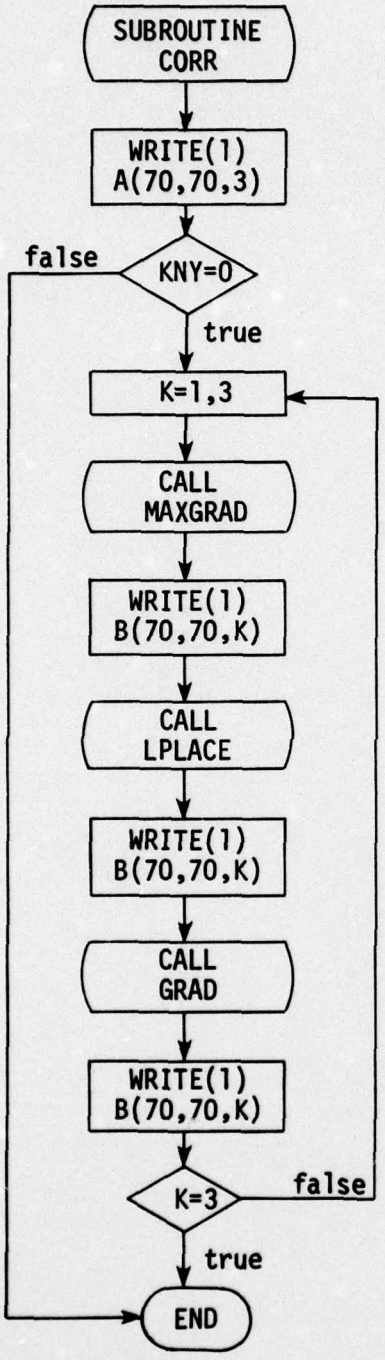

A equivalent to AG array
B equivalent to AGW array which is now used as a work array.

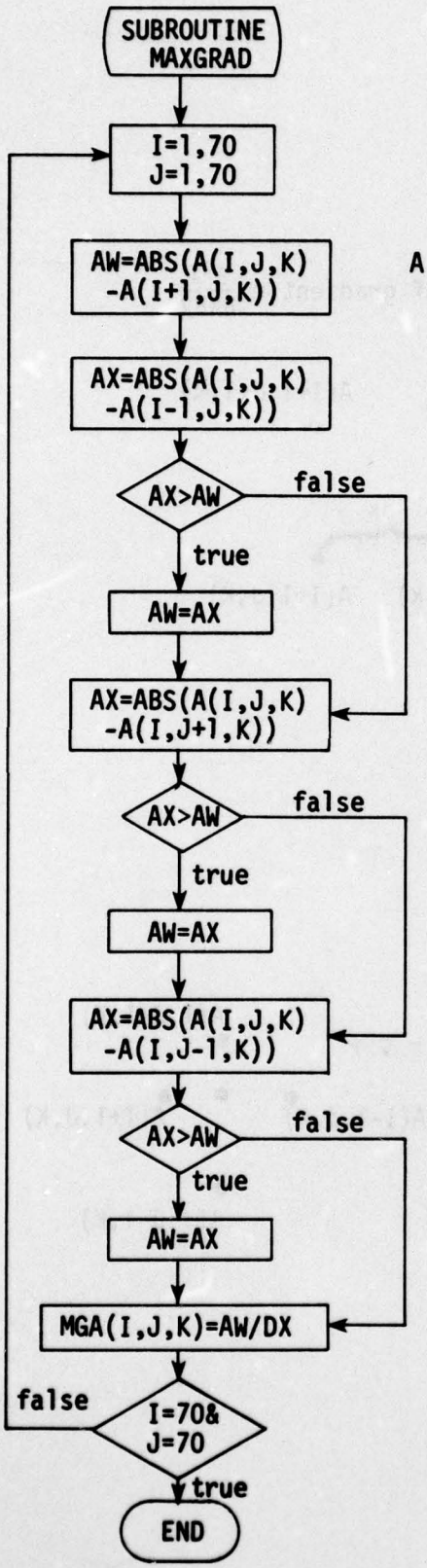

A - data array

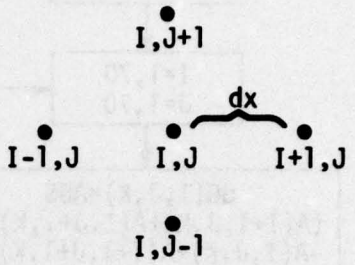

AW - maximum difference

MGA equivalent to B & AGW array
DX - distance between grid points KM

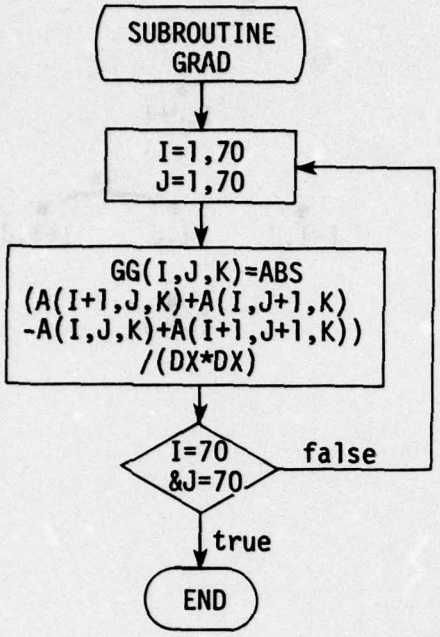

GG = gradient of gradient = $\frac{\partial^2 f}{\partial x \partial y}$

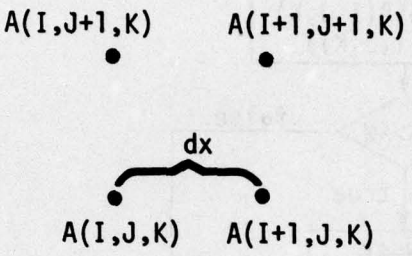

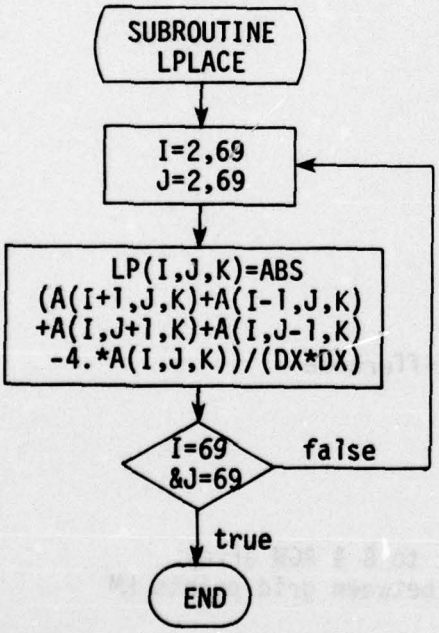

LP = Laplacian = $\nabla^2 f$

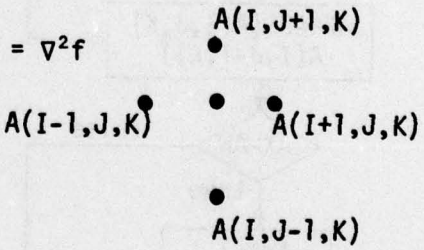

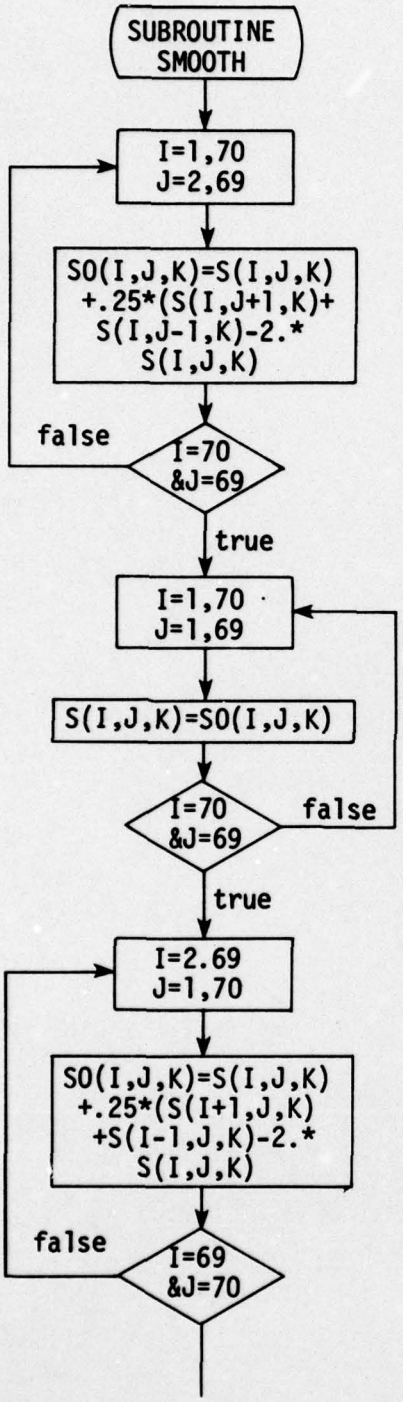

d

f(y-d) f(y) f(y+d)

$\bar{f}(y) = f(y) + .25[f(y+d) + f(y-d) - 2f(y)]$

Assume $f(y) = Ae^{iky}$ $\quad k = \frac{2\pi}{L}$

$\bar{f}(y) = Ae^{iky} + .25[Ae^{iky}e^{ikd} - 2Ae^{iky} + Ae^{iky}e^{ikd}]$

$= Ae^{iky}[1 + .25(e^{ihd} - 2 + e^{-ihd})]$

$= Ae^{iky}[1 + .25(-2 + 2\cos kd)]$

$= Ae^{iky}[1 - .5(1 - \cos kd)]$

$= Ae^{iky}[1 - .5(2\sin^2(\frac{kd}{2})]$

$= Ae^{iky}[1 - \sin^2(\frac{kd}{2})]$ $\quad k = \frac{2\pi}{L}$

$= f(y)[1 - \sin^2(\frac{kd}{2})]$ $\quad L$ = wavelength

Response func. $R^{(k)} = \frac{\bar{f}(y)}{f(y)} = 1 - \sin^2(\frac{kd}{2})$

$R(L) = 1 - \sin^2(\frac{\pi d}{L})$

Wavelength removed by application of this filter.

for R = 0

$1 - \sin^2(\frac{kd}{2}) = 0$

$\sin^2(\frac{kd}{2}) = 1$

$\frac{kd}{2} = \frac{\pi}{2}, \frac{3\pi}{2}, \frac{5\pi}{2} \ldots$

$k = \frac{2\pi}{L}$ = wave # $\quad L$ = wavelength

$\frac{d}{L} = \frac{\pi}{2}, \frac{3\pi}{2}, \frac{5\pi}{2} \ldots$

$L = 2d, \frac{2}{3}d, \frac{2}{5}d$

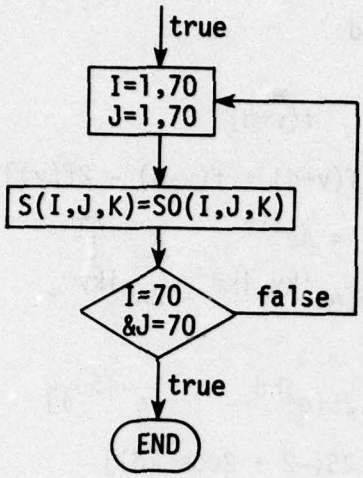
true
I=1,70
J=1,70
S(I,J,K)=SO(I,J,K)
I=70
&J=70
false
true
END

APPENDIX B

Data Presentation Procedures

The data includes Doppler and aircraft data for 1974, 1975 and 1976.

Time and derived gust velocity for each year's penetrations are archived on a single tape. Tom Jobson and Phil Bothwell wrote programs to build corresponding Doppler tapes containing only that Doppler data required for use in processing.

In order to obtain the aircraft position relative to the Doppler, the digital recorded WSR-57 and/or Doppler reflectivity data were first plotted using Calcomp plotter. These plots were aligned with the WSR-57 film data in order to minimize azimuthal or range variations due to scope synchro-drive lag. The aircraft position is shown on the film by the transponder [also called Identification Friend or Foe (IFF)] and the primary return or "skin-paint". These plane positions are traced on the plot. If a Doppler plot was not available for the same elevation angle as the WSR-57, the aircraft positions from the WSR-57 plot were directly transferred to a Doppler grid with no correction.

Using the set of points which represented the plane's position at 20 second intervals, a least squares fit of time vs. range and time vs. azimuth is used to compute the plane position at the midpoint of every five second interval from the beginning of the penetration to the end of the penetration.

For each five second interval thus determined, the Rough Rider turbulence data are scanned and the maximum recorded turbulence is found and stored.

Next, the Doppler data (reflectivity, radial velocity and standard deviation) are read from the Doppler tape and stored. From the Doppler data, the Laplacian of the velocity is computed. The gradient of the velocity is also computed, along with the gradient of the gradient and the reflectivity gradient. The "radial shear" is the second partial derenaline of the velocity over three radials. The "gate shear" is the second partial derivative of the velocity over three gates along the same radial!

For the aircraft position corresponding to the mid-point of each five second interval, the Doppler data for an area within 1 km of the aircraft is searched to find the maximum reflectivity, velocity, spectrum width, velocity gradient, gradient of the gradient, Laplacian, radial shear, and gate shear. These maximums are then printed out alongside the derived gust velocity.

For easy visual representation, a printer plotting program was developed which plots the maximum standard deviation, velocity gradient, gradient of the gradient, and the Laplacian, on the same graph as the derived gust velocity (Y axis) while each 5-second interval is represented on the X axis. For the average penetration speed this 5-second interval translates into a 1 km (0.5 n mi) interval.